Research Square

Preprints are preliminary reports that have not undergone peer review.
They should not be considered conclusive, used to inform clinical practice,
or referenced by the media as validated information.

A Graph Dynamics Optimizer with Lévy Diffusion and Opposition-Based Learning for Parameter Estimation of Triple-Diode Photovoltaic Models

Samah M. Elkholy
Kafrelshiekh University
Wala Azab
Kafrelshiekh University
Ahmed S. Bayoumi
ahmed.bayoumi@eng.kfs.edu.eg
Kafrelshiekh University
Arafa A. Nasif
Kafrelshiekh University
Manal E. Ali
Kafrelshiekh University

Article

Keywords: Graph Dynamics Optimizer, Lévy flight, Opposition-based learning, Photovoltaic parameter estimation, Triple diode model, Metaheuristic optimization

Posted Date: November 26th, 2026

DOI: https://doi.org/10.21203/rs.3.rs-11663139/v1

License: This work is licensed under a Creative Commons Attribution 4.0 International License.
Read Full License

Additional Declarations: No competing interests reported.

A Graph Dynamics Optimizer with Lévy Diffusion and Opposition-Based Learning for Parameter Estimation of Triple-Diode Photovoltaic Models

Samah M. Elkholy[1], Wala Azab[1], Ahmed S. Bayoumi[1 *], Arafa A. Nasif[1] , Manal E. Ali[1]

[1]Physics and Engineering Mathematics Department, Faculty of Engineering, Kafrelshiekh University, Kafrelshiekh, 33516, Egypt, walaa_ibrahim2011@kfs.edu.eg, ahmed.bayoumi@eng.kfs.edu.eg, manal.ali@eng.kfs.edu.eg, arafa.nasif@eng.kfs.edu.eg.
*Corresponding author: Ahmed S. Bayoumi

Abstract -

High-dimensional and multimodal optimization for estimating the parameters of advanced photovoltaic (PV) models is an unreliable task for many metaheuristics. We propose the Graph Dynamics Optimizer with L´evy Diffusion and Opposition Learning (GDO-LDOL) that embeds the population in a dynamic similarity-fitness graph, and replaces single-leader guidance with attraction to centrality-based hubs. Exploration (Laplacian diffusion with Lévy flights) and exploitation (neighbourhood message passing) are annealed over the run, supported by elitism, periodic opposition based learning and diversity restarts. The GDO-LDOL was applied on the 9, 10 and 11-parameter triple-diode (TDM), modified triple-diode (MTDM) and variable voltage-resistance triple-diode (VVR-TDM) models of R.T.C. France cell and compared with seven optimizers (PSO, APO, ARO, DO, SMA, ZOA, DOA) over 30 independent runs. It obtained the lowest minimum RMSE on all three models (7.425×10^{-4}, 7.405×10^{-4} and 7.252×10^{-4}) and the lowest mean RMSE: 19.3% lower than PSO on TDM, 8.0% lower than ARO on MTDM and 28.4% lower than PSO on VVR-TDM. The standard deviation on VVR-TDM was 2.68·10^(-5), and the maximum absolute current error of the best runs was no more than 1.41 mA. The results indicate that the graph-structured population dynamics can estimate the parameters of complex PV models accurately and stably.

Keywords : Graph Dynamics Optimizer; Lévy flight; Opposition-based learning; Photovoltaic parameter estimation; Triple diode model; Metaheuristic optimization

Notations

Symbol	Meaning
N	population size (number of search agents)
d	problem dimensionality (number of decision variables)
T	maximum number of iterations
lb, ub	lower and upper bound vectors of the search space ($\in \mathbb{R}^d$)
$x_i \in \mathbb{R}^d$	position (decision vector) of agent i
$X \in \mathbb{R}^{Nxd}$	population matrix, rows = agent positions

Symbol	Meaning
$f(\cdot)$	objective (fitness) function; here the I–V curve RMSE
F_i	fitness of agent i, $F_i = f(x_i)$
F_i^{safe}	positivity-shifted fitness used for edge-weight ratios
D_{ij}^2	squared Euclidean distance between agents i and j
σ_t	kernel bandwidth (population dispersion) at iteration t
K_{ij}	Gaussian spatial-similarity kernel between i and j
R_{ij}	fitness-ratio weighting factor between i and j
W_{ij}	full (dense) candidate edge weight, $W_{ij} = K_{ij} \cdot R_{ij}$
k	number of nearest neighbours retained per node
τ	edge-pruning threshold
p_r	small-world random rewiring probability
A	sparsified, symmetrized weighted adjacency matrix of graph G_t
s_i	weighted node strength (degree) of node i
C_i	hybrid centrality score of node i
α	centrality mixing coefficient
h, x_hub	index / position of the selected hub (most central) agent
D	diagonal strength matrix, $D = \mathrm{diag}(s_i)$
L	graph Laplacian, $L = D - A$
β_L	Lévy stability index (Mantegna's algorithm)
$Levy_i$	d-dimensional Lévy step vector drawn for agent i
γ	diffusion (Laplacian-flow) step size
β_t	time-decayed hub-attraction coefficient
P_diff(t)	iteration-dependent probability of the exploration branch
η_{ij}	normalized message-passing weight from neighbour j to i
n_elite	number of elite agents preserved per iteration

1. Introduction

The transition to renewable energy sources has become a key strategic strategy to meet rising global energy demand and the accompanying environmental and economic challenges arising from an over-dependence on fossil fuels [1,2]. In this context, the solar PV is the key as it is a mature and scalable technology with low operating costs and easy integration into a range of energy grids from small residential to large industrial plants [3–5].

Accurate mathematical modelling of PV cells and modules is a prerequisite for optimal use of PV cells and modules [6,7] . The models are used for simulation of the electrical performance under different operating conditions, design of optimal Maximum Power Point Tracking (MPPT) systems and evaluation of the efficiency of the system before actual installation[8]. However, the accuracy of such models is heavily dependent on the correct estimation of un-

known electrical parameters, which becomes increasingly complex as the model sophistication increases.

Single and double diode models are relatively simplified representations, while more advanced models such as the Three Diode Model (TDM) [9], the Modified Three Diode Model (MTDM) and the VVR-TDM [10] provide greater accuracy in simulating subtle physical phenomena such as edge leakage and voltage-dependent shunt resistance. However, these advanced models increase the number of parameters to be estimated, making the estimation process a high dimensional, non-linear optimization problem with several local optima that are hard to resolve by conventional analytical or numerical methods [11,12].

Researchers have resorted to metaheuristic optimization algorithms as good tools to explore the solution space and to manage its non-linear and non-convex nature in an effort to solve this problem [13].

Over the past three decades, a broad and diverse family of such algorithms has been proposed and applied to PV parameter estimation and related engineering problems[14] , including Particle Swarm Optimization (PSO) [15], Genetic Algorithm (GA)[16] , Differential Evolution (DE) [17], Grey Wolf Optimizer (GWO) [18], Whale Optimization Algorithm (WOA) [19] , [20] (SSA), Harris Hawks Optimization (HHO)[21] , [22] (SCA), Ant Lion Optimizer (ALO) [23], Moth-Flame Optimization (MFO)[24] , Cuckoo Search (CS)[25] , [26] (BA), Firefly Algorithm (FA) [27], Artificial Bee Colony (ABC)[28] , Teaching-Learning-Based Optimization (TLBO)[29] , Slime Mould Algorithm (SMA)[30] , Artificial Protozoa Optimizer (APO) [31], Artificial Rabbits Optimization (ARO)[32] , Dandelion Optimizer (DO) [33], Zebra Optimization Algorithm (ZOA)[34] , and the Dream Optimization Algorithm (DOA)[35] . However, many of these algorithms still suffer from well-known problems, such as the entrapment in local optima, the imbalance between exploration and exploitation phases and the slow convergence rate in case of highly complex models such as TDM, MTDM and VVR-TDM.

To fill this gap, this paper suggests the use of graph theory [36] as a new structural framework in the optimization process through the proposed algorithm called “Graph Dynamics Optimizer”. Two complementary mechanisms are introduced to enhance this algorithm: Lévy diffusion [37], to improve the algorithm’s ability to perform wide exploratory leaps and to avoid premature convergence; opposition-based learning, to enhance the convergence by increasing the initial and intermediate coverage of the search space. This combination is to get a better trade-off between exploration and exploitation, which may be better than the traditional algorithms in accuracy and stability of parameter estimation. The main contribution of this work is the application of the proposed algorithm to three of the most complex diode models, namely TDM, MTDM, and VVR-TDM, and the performance of a thorough comparative analysis of their performance in terms of estimation accuracy, convergence speed, and statistical stability over multiple runs. This gives more insight into the applicability of each model for practical applications and provides a methodological framework that can be extended to parameter

estimation problems in other photovoltaic power systems. The overall research framework is illustrated in Figure 1.

The research workflow are illustrated in flowchart below can be summarized as follows:

1. A novel graph-based metaheuristic framework. We propose GDO-LDOL, which departs from classical leader-following swarm schemes by embedding the population in a dynamic, weighted similarity–fitness graph at every iteration, replacing single-leader guidance with topological hub-based attraction.
2. Dual-operator search mechanism. Two graph-topological operators are introduced — a Laplacian-diffusion/Lévy-flight exploration operator and a neighbourhood message-passing exploitation operator — with their relative influence annealed over the run to shift the search from broad exploration to focused exploitation.
3. Multi-mechanism stabilization. The algorithm integrates elitism, greedy selection, success-rate-based step-size adaptation, periodic opposition-based learning, and stagnation-triggered diversity restarts to guard against premature convergence and loss of diversity.
4. Application to three high-complexity diode models. GDO-LDOL is applied, for the first time in this combined form, to parameter estimation of TDM, MTDM, and VVR-TDM — among the most parameter-rich and physically detailed PV models in the literature.
5. Comprehensive comparative validation. The proposed algorithm is benchmarked against seven state-of-the-art optimizers (Artificial Protozoa Optimizer (APO), Artificial Rabbits Optimization (ARO), Dandelion Optimizer (DO), Dream Optimization Algorithm (DOA), Particle Swarm Optimization (PSO), Zebra Optimization Algorithm (ZOA), Slime Mould Algorithm (SMA) on the standard R.T.C. France solar cell dataset over 30 independent runs, demonstrating superior accuracy, convergence speed, and statistical robustness across all three models.

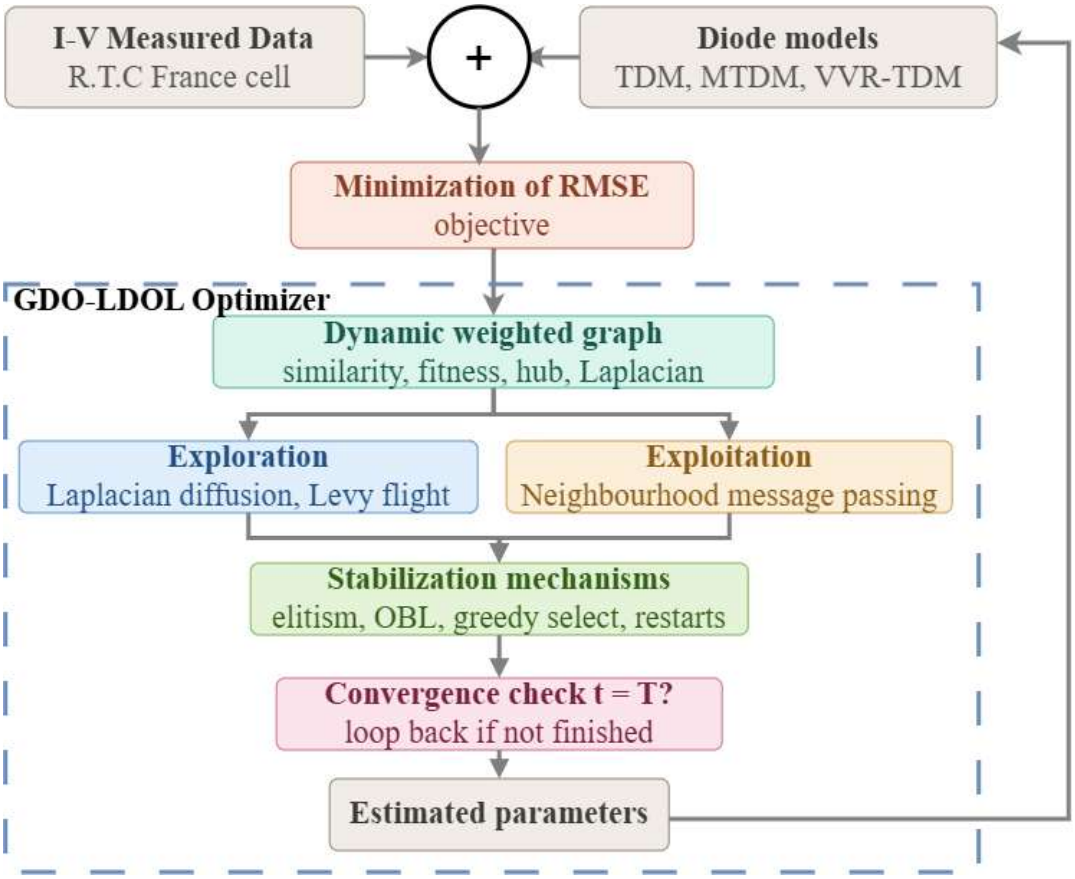


Figure 1. The research flowchart.

The rest of the paper is structured in the following manner: Section 2 provides the mathematical formulation of the TDM, and MTDM, VVR-TDM together with the objective function. Section 3 shows mathematical formulation of GDO-LDOL Optimization Algorithm. Section 4 gives the experimental results and comparison analysis. Section 5 concludes the paper with important findings and future work.

2. Methodology

This section describes the photovoltaic (PV) models and the optimization problem addressed in this study. Three diode-based equivalent circuits of increasing complexity are considered: the Triple Diode Model (TDM), the Modified Triple Diode Model (MTDM), and the Variable Voltage-Resistance Triple Diode Model (VVR-TDM). Their mathematical formulations are presented in Section 2.1, followed by the objective function used to quantify the mismatch between measured and simulated I–V data (Section 2.1.3) and the experimental conditions and algorithm settings (Section 2.1.4). The unknown parameters of each model are then identified by the proposed GDO-LDOL algorithm (Section 3) and compared with seven state-of-the-art optimizers.

2.1. Photovoltaic Modeling

The electrical behaviour of a PV cell is commonly represented by equivalent circuits in which a photo-generated current source is connected in parallel with one or more diodes and a shunt resistance, and in series with a series resistance. The photo-generated current I_{ph} is proportional to the incident irradiance, the diodes describe the recombination and diffusion mechanisms of the p–n junction, R_s lumps the contact, bulk, and metallization resistances, and R_{sh} represents leakage paths across the junction.

Single- and double-diode models are widely used because of their simplicity, but they cannot fully reproduce additional loss mechanisms such as recombination at grain boundaries, peripheral leakage, and voltage-dependent resistive effects. Adding further diodes and resistive elements improves the fit to measured I–V data, but increases the number of unknown parameters and makes their identification a harder, multimodal optimization problem. In this work, three three-diode formulations are studied, with 9, 10, and 11 unknown parameters for the TDM, MTDM, and VVR-TDM, respectively. In all equations, q is the electron charge (1.602×10^{-19} C), k (or k_B) is the Boltzmann constant (1.381×10^{-23} J/K), and T is the cell temperature in kelvin (303.15 K in this study).

2.1.1. Triple Diode Model

The TDM extends the double-diode model by adding a third diode in parallel, which accounts for recombination in defect-rich regions, grain boundaries, and peripheral leakage that the first two diodes do not capture. As shown in Figure 2, the circuit consists of a photo-generated current source Iph, three parallel diodes with saturation currents I_{sd1}, I_{sd2}, and I_{sd3} and ideality factors n_1, n_2, and n_3, a shunt resistance R_{sh}, and a series resistance Rs. The terminal current is given by Eq. (1), where $I_{sh} = (V + I\cdot R_s)/R_{sh}$ is the shunt current. The model therefore has nine unknown parameters: {I_{ph}, I_{sd1}, I_{sd2}, I_{sd3}, R_s, R_{sh}, n_1, n_2, n_3}.

$$I = I_{ph} - I_{sh} - \sum_{j=1}^{3} I_{sdj} = I_{ph} - \frac{V+IR_s}{R_{sh}} - \sum_{j=1}^{3} I_{ssdj}\left[exp\left(\frac{q(V+IR_s)}{n_j kT}\right) - 1\right] \quad (1)$$

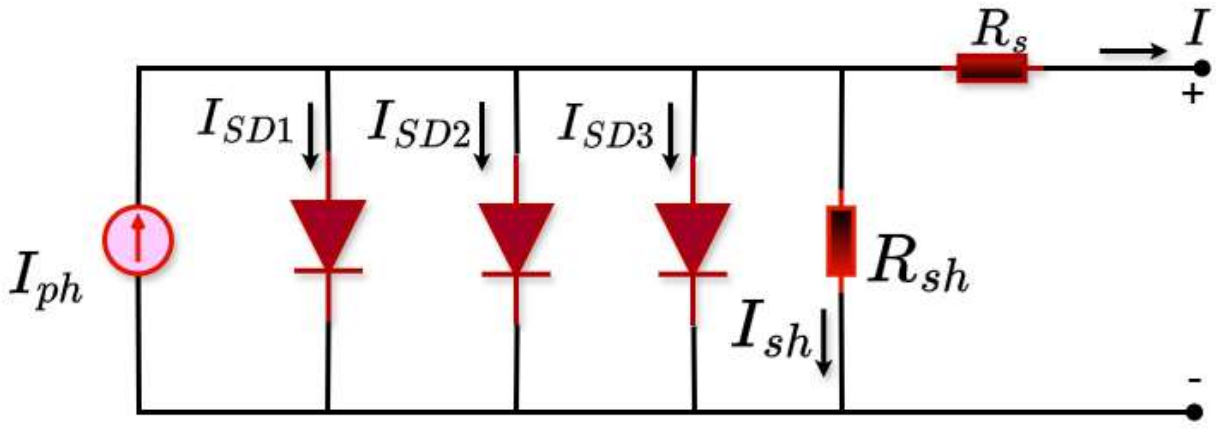


Figure 2. Equivalent circuit of TDM

2.1.2. Modified Triple Diode Model (M TDM)

The MTDM modifies the third branch of the TDM by adding a resistance R_m in series with the third diode[38] . This resistance represents the additional resistive loss in the path of the third diode, so the voltage across that diode is reduced by the drop $I_{sd3} \cdot R_m$, as seen in the exponent of the third term in Eq. (2). The first two diodes are unchanged from the TDM. As shown in Figure 3, the model has ten unknown parameters: { I_{ph}, I_{sd1}, I_{sd2}, I_{sd3}, R_s, R_{sh}, n_1, n_2, n_3, R_m} [38] . The extra parameter raises the dimensionality and the non-linearity of the estimation problem.

$$I = I_{ph} - \sum_{i=1}^{2} I_{sdi}\left[exp\left(\frac{q(V+IR_s)}{N_i KT}\right) - 1\right] - I_{sd3}\left[\exp\left(\frac{q(V+IR_S - I_{sd3}R_m)}{N_3 KT}\right) - 1\right] - \frac{V+IR_S}{R_{sh}} \quad \textbf{(2)}$$

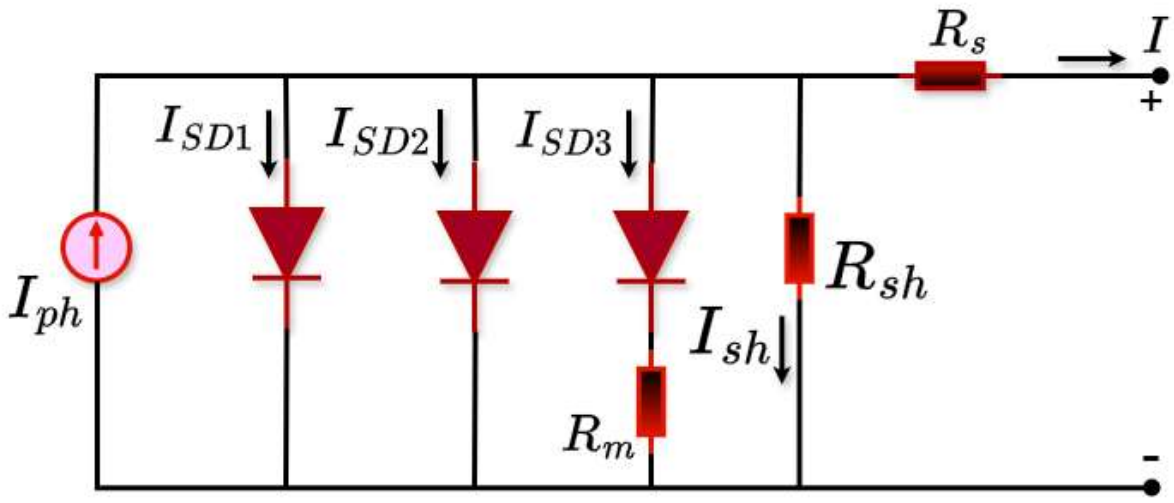


Figure 3. Equivalent circuit of MTDM

2.1.3. Variable voltage resistances Triple Diode Model (VVR TDM)

In the TDM and MTDM, the series and shunt resistances are treated as constants. In practice, they vary with the operating voltage[39] . The VVR-TDM captures this by modelling both resistances as linear functions of the terminal voltage: $R_s(V) = R_{so}(1 + K_s \cdot V)$ and $R_p(V) = R_{po}(1 + K_p \cdot V)$, where R_{so} and R_{po} are the resistances at zero voltage and Ks and Kp are voltage coefficients. As shown in Figure 4, the model keeps three parallel diodes and has eleven unknown parameters: { I_{ph}, I_{sd1}, I_{sd2}, I_{sd3}, R_s, R_{sh}, n_1, n_2, n_3, R_{so}, R_{po}, K_s, K_p}. Because the resistive terms are coupled to the voltage, the resulting objective function is the most non-linear and numerically demanding of the three models.

$$I = I_{ph} - \sum_{i=1}^{3} I_{si}\left[\exp\left(\frac{q(V+R_{so}(1+K_S \cdot V) \cdot I)}{(n_i) \cdot k_B \cdot T}\right) - 1\right] - \frac{V+R_{so}(1+K_S \cdot V) \cdot I}{R_{po}(1+K_p \cdot V)}, \quad (3)$$

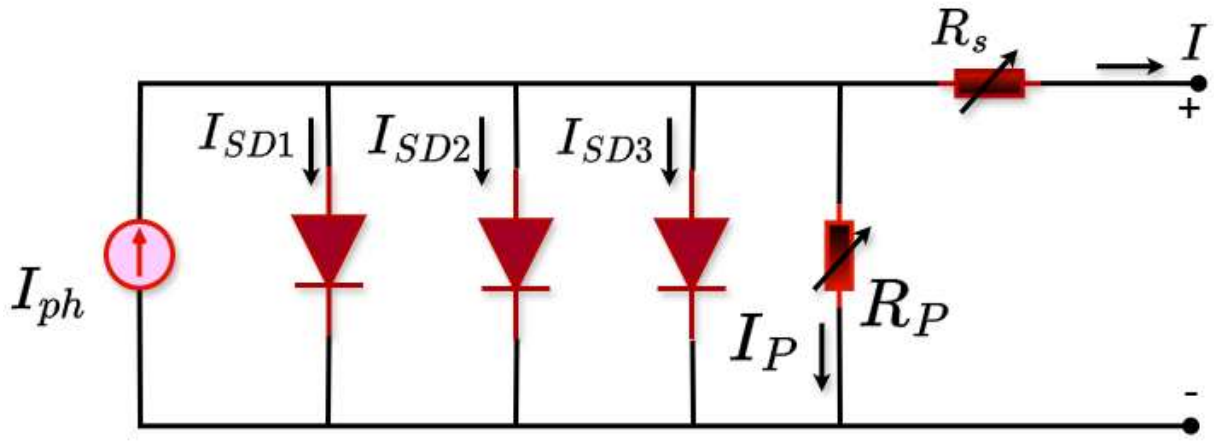


Figure 4. Equivalent circuit of VVR-TDM

2.2 Objective Function

The Objective Function (OF) shows the least difference among the estimated and experimental data when the ideal parameter values are used. The majority of algorithms, employ the total RMSE as their assessment criterion. The RMSE may also be used to assess the disparity between predicted and actual results. So, RMSE is nominated as the OF as shown in Eq. (4)

$$OF(X) = RMSE(X) = \sqrt{\frac{1}{M} \times \sum_{d=1}^{M} f_d(V_L, I_L, X)^2} \tag{4}$$

where X stands for the vector holding the to be estimated unknown parameters and M is the total number of experimental I-V data points. the function $f_M(V_L,I_L,X)$ represents the error between the estimated current (I_{est}) and the current measured (I_t). Specifically, for the single diode model, the function $f_{SM}(V_L,I_L,X)$ is derived by subtracting Eq.(1) from the measured current value (I_t), as shown in Eq.(5) Similarly, Eq.(6) were obtained by using Eq.(2) , and (7) respectively, instead of Eq.(3)

For TDM:

$$\begin{cases} f(\mathrm{V}, I, X) = I_{ph} - I_{sd1}\left[exp\left(\frac{\mathrm{V}+\mathrm{I}R_s}{n_1 kT/q}\right) - 1\right] \\ -I_{sd2}\left[exp\left(\frac{\mathrm{V}+\mathrm{I}R_s}{n_2 kT/q}\right) - 1\right] - I_{sd3}\left[exp\left(\frac{\mathrm{V}+\mathrm{I}R_s}{n_3 kT/q}\right) - 1\right] - \frac{\mathrm{V}+\mathrm{I}R_s}{R_{sh}} - \mathrm{I}, \\ X = \{I_{ph}, I_{sd1}, I_{sd2}, I_{sd3}, R_s, R_{sh}, n_1, n_2, n_3\} \end{cases} \tag{5}$$

For MTDM:

$$\begin{cases} f(\mathrm{V}, I, X) = \\ I_{Ph} - I_{sd1}\left[\exp\left(\frac{q(V+IR_S)}{N_1 KT}\right) - 1\right] - I_{sd2}\left[\exp\left(\frac{q(V+IR_S)}{N_2 KT}\right) - 1\right] - \\ I_{sd3}\left[\exp\left(\frac{q(V+IR_S - I_{sd3}R_m)}{N_3 KT}\right) - 1\right] - \frac{V+IR_S}{R_{sh}} - \mathrm{I}, \\ X = \{I_{ph}, I_{sd1}, I_{sd2}, I_{sd3}, R_s, R_{sh}, n_1, n_2, n_3, R_m\} \end{cases} \quad (6)$$

For VVR - TDM:

$$\begin{cases} f(\mathrm{V}, I, X) = \\ I = I_{ph} - I_{s1}\left[\exp\left(\frac{q(V+R_{so}(1+K_s \cdot V)\cdot I)}{(n_1)\cdot k_B \cdot T}\right) - 1\right] - I_{s2}\left[\exp\left(\frac{q(V+R_{so}(1+K_s \cdot V)\cdot I_s)}{(n_2)\cdot k_B \cdot T}\right) - 1\right] \\ -I_{s3}\left[\exp\left(\frac{q(V+R_{so}(1+K_s \cdot V)\cdot I)}{(n_3)\cdot k_B \cdot T}\right) - 1\right] - \frac{V+R_{so}(1+K_s \cdot V)\cdot I}{R_{po}(1+K_p \cdot V)} - I, \\ X = \{I_{ph}, I_{sd1}, I_{sd2}, I_{sd3}, n_1, n_2, n_3,\ R_{s0}, R_{PO}\ ,\ K_s, K_P\} \end{cases} \quad (7)$$

2.1.4. Parameter Setting

Experimental I–V data were taken from the commercial 57 mm diameter R.T.C. France silicon solar cell, a standard benchmark in PV parameter estimation[40] . The cell was measured at an irradiance of 1000 W/m² and a temperature of 33 °C. Its main specifications are listed in Table 1, and the 26 measured voltage–current pairs used as the fitting data are listed in Table 3.

To make the comparison fair, all eight algorithms (the proposed GDO-LDOL, PSO, APO, ARO, DO, SMA, ZOA, and DOA) were run under identical computational conditions, as shown in Table 2: a population size of 30, a maximum of 1000 iterations, and 30 independent runs for each model.

Table 1. Specifications of commercial R.T.C Solar Cell

57 mm Diameter R.T.C France Solar Cell	
Operation Temperature (K)	303.15
Operation radiation (W/m²)	1000
Maximum power (Pmpp) (W)	0.3101
Voltage at MPP (Vmpp) (V)	0.4507
Current at MPP (Impp) (A)	0.6880
Open circuit voltage (Voc) (V)	0.5727
Short circuit current (Isc) (A)	0.7605

Table 2. The optimization algorithm setting.

Parameter Settings	
Independent run time	30
Population size	30
Iteration time	1000

Table 3. Experimental I-V Data for R.T.C. France Solar Cell (at 33°C)

Index	Experimental Voltage (V)	Experimental Current (A)
0	-0.2057	0.764000
1	-0.1291	0.762000
2	-0.0588	0.760500
3	0.0057	0.760500
4	0.0646	0.760000
5	0.1185	0.759000
6	0.1678	0.757000
7	0.2132	0.757000
8	0.2545	0.755500
9	0.2924	0.754000
10	0.3269	0.750500
11	0.3585	0.746500
12	0.3873	0.738500
13	0.4137	0.728000
14	0.4373	0.706500
15	0.4590	0.675500
16	0.4784	0.632000
17	0.4960	0.573000
18	0.5119	0.499000
19	0.5265	0.413000
20	0.5398	0.316500
21	0.5521	0.212000
22	0.5633	0.103500
23	0.5736	-0.010000
24	0.5833	-0.123000
25	0.5900	-0.210000

3. GDO-LDOL Optimization Algorithm

Graph Dynamics Optimizer with Lévy Diffusion and Opposition Learning (GDO-LDOL) is a population-based metaheuristic that departs from classical swarm-leader-following schemes by embedding the population in a dynamic, weighted graph at every iteration. Rather than moving agents toward a single "best" leader, GDO-LDOL (i) builds a similarity–fitness graph over the current population, (ii) identifies a topologically and fitness-central hub agent through a graph-centrality measure, and (iii) updates each agent through one of two graph-topological operators: a Laplacian-diffusion / Lévy-flight exploration operator, or a neighbourhood message-passing exploitation operator. The balance between the two operators is annealed over the run, and the search is further stabilised by elitism, greedy selection, success-based step-size adaptation, periodic opposition-based learning, and stagnation-triggered diversity restarts.

Figure 5 illustrates this mechanism schematically: the population is embedded as a weighted graph within the feasible search space, with edge width and opacity encoding the pairwise similarity–fitness weight Wij. The agent of highest hybrid centrality is selected as the hub (highlighted node), around which the two update operators act — a Lévy-flight step that diffuses an agent's position while biasing it toward the hub (exploration), and a neighbourhood message-passing step that pulls an agent toward a weighted average of its graph neighbours (exploitation).

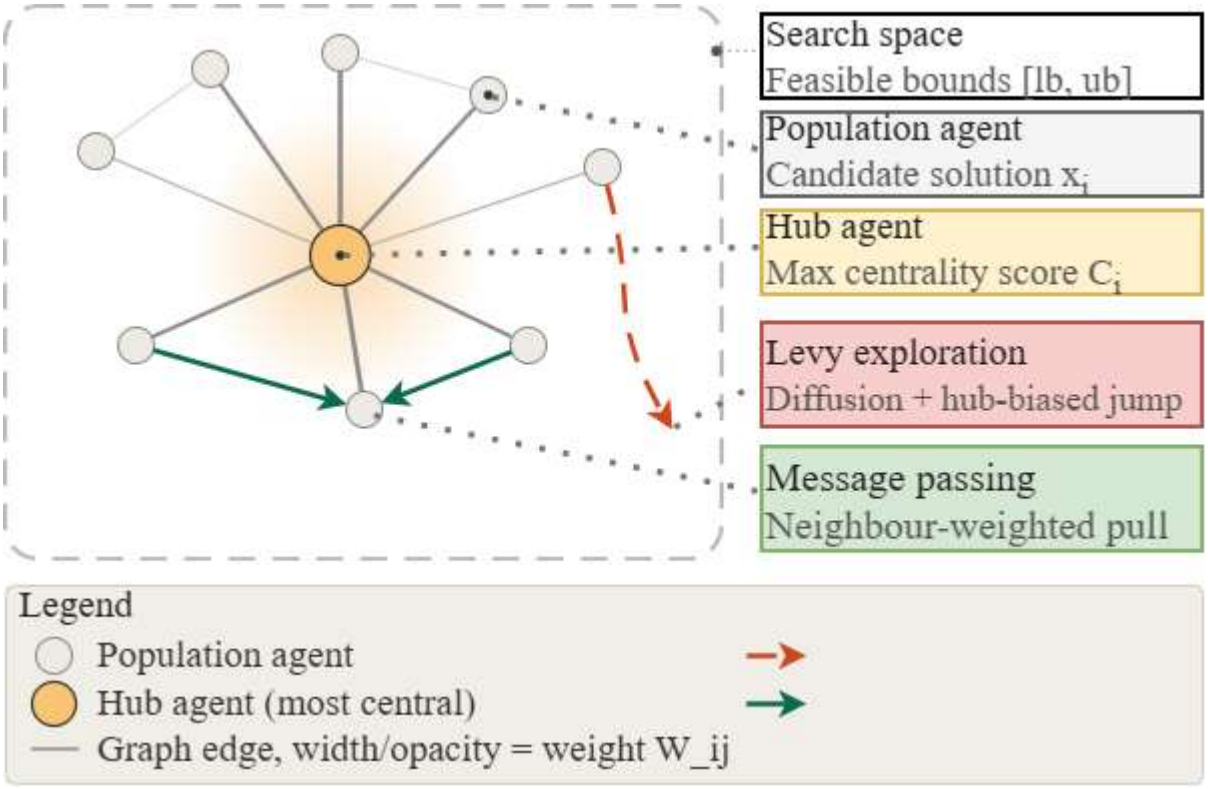


Figure 5. Schematic illustration of the GDO-LDOL search mechanism.

3.1 Population Initialization

The population X = {x_1, x_2, …, x_N} is initialized by uniform random sampling within the search-space bounds, independently for every agent i and every dimension j:

$$x_{i,j}^{(0)} = lb_j + r_{i,j}\,(ub_j - lb_j)\,, \qquad r_{i,j} \sim U(0,1) \tag{8}$$

The fitness of every agent is then evaluated once, $F_i = f(x_i)$, i = 1,…,N, and the incumbent global best (x*, F*) is set to the fittest agent.

3.2 Positivity-Shifted ("Safe") Fitness

Because the graph-edge weights below use a fitness ratio F_j / F_i, which is only well defined for strictly positive, order-preserving fitness values, the raw fitness vector is first shifted to be strictly positive while preserving rank and relative differences:

$$s = \min\left\{0,\ \min_i F_i\right\} \tag{9}$$

$$F_i^{\text{safe}} = F_i - s + \varepsilon \tag{10}$$

with a small constant $\varepsilon = 10^{-12}$ preventing division by zero in Eq. (6)–(7).

3.3 Similarity Kernel and Fitness-Ratio Edge Weights

For every ordered pair (i, j) the pairwise squared Euclidean distance in decision space is combined with a Gaussian spatial-similarity kernel and a clipped fitness-ratio factor to form a dense candidate weight matrix:

$$D_{ij}^2 = \|x_i - x_j\|^2 \tag{11}$$

$$K_{ij} = \exp\left(-\frac{D_{ij}^2}{2\sigma_t^2 + \varepsilon}\right) \tag{12}$$

$$R_{ij} = \text{clip}\left(\frac{F_j^{\text{safe}}}{F_i^{\text{safe}} + \varepsilon},\ 0,\ R_{\max}\right) \tag{13}$$

$$W_{ij} = K_{ij} \times R_{ij}, \qquad W_{ii} = 0 \tag{14}$$

σ_t is the time-varying kernel bandwidth (Section 3.9) and R_max is a clipping ceiling (default 5) that prevents extreme fitness disparities from producing numerically unstable edge weights. Note that W_{ij} is, in general, asymmetric because $R_{ij} \neq R_{ji}$.

3.4 k-Nearest-Neighbour Sparsification and Pruning

The dense candidate graph is restricted to a k-nearest-neighbour (k-NN) graph in decision space, and weak edges are pruned with a threshold τ:

$$\mathcal{N}_k(i) = \{\, k \text{ indices } j \text{ with smallest } D_{ij}^2 \,\} \tag{15}$$

$$A_{ij} = \begin{cases} W_{ij} & \text{if } j \in \mathcal{N}_k(i) \text{ and } W_{ij} \geq \tau \\ 0 & \text{otherwise} \end{cases} \tag{16}$$

3.5 Small-World Rewiring and Symmetrization

To preserve long-range information flow (avoiding a purely local k-NN topology), each node rewires to a uniformly random node with probability p_r, keeping the larger of the existing and candidate weight; the resulting directed graph is finally symmetrized to obtain the undirected adjacency matrix A used by the remaining operators:

$$A_{ij} \leftarrow \max(A_{ij}, W_{ij}) \quad \text{w.p. } p_r, \quad \forall j \sim U\{1, \ldots, N\} \tag{17}$$

$$A_{ij}^{\text{sym}} = \max(A_{ij},\, A_{ji}) \tag{18}$$

3.6 Node Strength and Hybrid Centrality

The weighted node degree (strength) and a hybrid topological/fitness centrality score are computed for every agent, and the most central agent is selected as the diffusion hub:

$$s_i = \sum_j A_{ij}^{\text{sym}} \tag{19}$$

$$C_i = \alpha \, \frac{s_i}{\max_i s_i + \varepsilon} \; + \; (1 - \alpha) \, \frac{\min_i F_i^{\text{safe}}}{F_i^{\text{safe}} + \varepsilon} \tag{20}$$

$$h = \arg\max_i C_i, \qquad x_{\text{hub}} = x_h \tag{21}$$

$\alpha \in [0,1]$ (default 0.5) balances topological prominence (normalized strength) against relative fitness quality in the centrality score.

3.7 Graph Laplacian

The (combinatorial) graph Laplacian of the symmetrized graph drives the diffusion component of the exploration operator:

$$D = \text{diag}(s_1, \ldots, s_N), \qquad L = D - A^{\text{sym}} \tag{22}$$

$$(LX)_i = s_i x_i - \sum_j A_{ij}^{\text{sym}} \, x_j = \sum_j A_{ij}^{\text{sym}} \, (x_i - x_j) \tag{23}$$

i.e. row i of L X aggregates the (weighted) deviation of agent i from each of its graph neighbours.

3.8 Lévy Flight (Mantegna's Algorithm)

Heavy-tailed exploration steps are generated with Mantegna's algorithm for a Lévy-stable random walk of index β_L (default 1.5):

$$\sigma_u = \left[\frac{\Gamma(1+\beta_L)\,\sin\left(\frac{\pi\beta_L}{2}\right)}{\Gamma\left(\frac{1+\beta_L}{2}\right)\,\beta_L\,2^{(\beta_L-1)/2}} \right]^{1/\beta_L} \tag{24}$$

$$u \sim \mathcal{N}(0, \sigma_u^2), \qquad v \sim \mathcal{N}(0,1), \qquad \text{Levy} = \frac{u}{|v|^{1/\beta_L}} \tag{25}$$

u and v are drawn independently for each of the d dimensions, giving a d-dimensional step vector Levy_i per agent.

3.9 Iteration-Adaptive Control Parameters

Three control parameters are linearly / multiplicatively annealed over the run of T iterations, shifting the search from broad exploration toward local exploitation:

$$P_{\text{diff}}(t) = 0.9 - 0.8\,\frac{t}{T} \tag{26}$$

$$\beta_t = \beta\left(1 - \frac{t}{T}\right) \tag{27}$$

$$\sigma_0 = \frac{1}{N^2}\sum_{i,j}\|x_i - x_j\|^2 + \varepsilon \quad \text{(computed once, at } t = 0) \tag{28}$$

$$\sigma_t = \max\left\{\ \sigma_0\left(1 - 0.8\,\frac{t}{T}\right),\ 10^{-8}\ \right\} \tag{29}$$

Here β is the (fixed) initial hub-attraction gain and P_diff(t) is the probability that a given agent, at iteration t, follows the exploration branch rather than the exploitation branch (Section 3.10); both decay from a broad, diffusion-favouring regime toward a narrower, message-passing-favouring regime as t → T.

3.10 Agent Update Rule

At every iteration, each agent independently draws u_i ~ U(0,1) and follows one of two branches.

Exploration branch (u_i < P_diff(t)): Laplacian diffusion + Lévy-modulated hub attraction.

$$x_i^{\text{new}} = x_i + \gamma\,(LX)_i + \beta_t\,(x_{\text{hub}} - x_i) \odot \text{Levy}_i \qquad \text{[exploration]} \tag{30}$$

where $\odot$ denotes the element-wise (Hadamard) product with the d-dimensional Lévy step vector.

Exploitation branch (u_i ≥ P_diff(t)): neighbourhood message passing.

For agent i with neighbour set $\mathcal{N}(i) = \{j : A_ij\text{^sym} > 0\}$, if $\mathcal{N}(i) \neq \emptyset$:

$$\eta_{ij} = \frac{A_{ij}^{\text{sym}}}{\sum_{k \in \mathcal{N}(i)} A_{ik}^{\text{sym}} + \varepsilon}, \qquad j \in \mathcal{N}(i) \tag{31}$$

$$m_i^{\text{avg}} = \sum_{j \in \mathcal{N}(i)} \eta_{ij}\,(x_j - x_i) \tag{32}$$

$$j^* = \arg\min_{j \in \mathcal{N}(i)} F_j, \qquad m_i^{\text{best}} = x_{j^*} - x_i \tag{33}$$

$$x_i^{\text{new}} = x_i + m_i^{\text{avg}} + 0.5\, m_i^{\text{best}} \qquad \text{[exploitation]} \tag{34}$$

If $\mathcal{N}(i) = \emptyset$ (an isolated node after pruning), the agent is left unchanged: $x_i\text{^new} = x_i$. In both branches the candidate position is finally clipped component-wise to the feasible box:

$$x_i^{\text{new}} = \min\big(\max(x_i^{\text{new}}, lb),\, ub\big) \tag{35}$$

3.11 Greedy Selection

$$x_i \leftarrow \begin{cases} x_i^{\text{new}} & \text{if } f(x_i^{\text{new}}) < F_i \\ x_i & \text{otherwise} \end{cases} \tag{36}$$

3.12 Success-Rate-Based Adaptation of the Diffusion Step γ

Let the success rate be the fraction of agents improved by greedy selection at iteration t:

$$p_s(t) = \frac{1}{N} \sum_{i=1}^{N} \mathbf{1}[F_i^{\text{new}} < F_i] \tag{37}$$

$$\gamma \leftarrow \begin{cases} 1.05\,\gamma & \text{if } p_s(t) > 0.20 \\ 0.95\,\gamma & \text{otherwise} \end{cases} \tag{38}$$

$$\gamma \leftarrow \text{clip}(\gamma,\ \gamma_{\min},\ \gamma_{\max}) \tag{39}$$

3.13 Periodic Opposition-Based Learning (OBL)

Every 50 iterations, an opposite population is generated and greedily accepted if it improves fitness — a low-cost mechanism for escaping local regions of the search space:

$$x_i^{\text{opp}} = \text{clip}(lb + ub - x_i,\ lb,\ ub) \tag{40}$$

$$x_i \leftarrow x_i^{\text{opp}} \quad \text{if } f(x_i^{\text{opp}}) < F_i \tag{41}$$

3.14 Diversity Monitoring and Stagnation Restart

Population diversity is monitored via the mean per-dimension standard deviation; if the swarm has collapsed, the worst 80% of agents (by fitness rank) are re-initialized uniformly at random:

$$\text{Div}(t) = \frac{1}{d}\sum_{j=1}^{d} \text{std}_i(x_{ij}) \tag{42}$$

$$\text{if } \text{Div}(t) < 10^{-4}: \text{ reinitialize the worst } \lfloor 0.8N \rfloor \text{ agents} \tag{43}$$

3.15 Elitism

Before the update step, the top n_elite agents (by fitness) are cached; after selection, adaptation, OBL and diversity restart, they overwrite the current worst n_elite agents, guaranteeing that the best solutions found so far are never lost:

$$n_{\text{elite}} = \max(1,\ \lfloor 0.05\,N \rfloor) \tag{44}$$

3.16 Global Best Update

$$F^* = \min\left(F^*,\ \min_i F_i\right), \qquad x^* = \arg\min \text{ over all evaluated agents} \tag{45}$$

The best fitness found up to and including iteration t is logged as Convergence_curve[t] = F*, yielding the monotone convergence trace reported in the results section.

3.17. Pseudocode

Algorithm 1 lists the GDO procedure exactly as implemented, including the elitism, greedy-selection, opposition-based-learning and diversity-restart mechanisms of Sections 3.11–3.15.

Algorithm 1: Graph Dynamics Optimizer (GDO)

```
Input : N (agents), T (max. iterations), lb, ub, d, objective f(·)
        alpha, k, sigma (opt. fixed bandwidth), tau, p_r, R_max,
        gamma0, beta, beta_L (Levy index)
Output: x*, F*, Convergence_curve[1..T]
n_elite <- max(1, floor(0.05 N));  gamma <- gamma0                  Eq. (44)
X <- Initialize(N, d, lb, ub)                                       Eq. (8)
F[i] <- f(X[i])  for i = 1..N
(x*, F*) <- (X[argmin F], min F)
sigma0 <- None
for t = 1 to T do
   elite_idx <- indices of the n_elite smallest F                   Sec. 3.15
   (X_elite, F_elite) <- (X[elite_idx], F[elite_idx])
   P_diff(t) <- 0.9-0.8(t/T);  beta_t <- beta(1-t/T)                Eq. (26)-(27)
   F_safe <- SafeFitness(F)                                         Eq. (9)-(10)
   if sigma0 is None: sigma0 <- MeanPairwiseDist(X)                 Eq. (28)
   sigma_t <- max(sigma0(1 - 0.8 t/T), 1e-8)                        Eq. (29)
   A <- BuildGraph(X,F_safe,sigma_t,tau,k,p_r,R_max)                Eq. (11)-(18)
   s <- RowSum(A);  C <- Centrality(s, F_safe, alpha)               Eq. (19)-(20)
   x_hub <- X[argmax C];  L <- diag(s) - A                          Eq. (21)-(22)
   for i = 1 to N do                                                Sec. 3.10
      if rand() < P_diff(t) then                                    EXPLORATION
         Levy_i <- MantegnaLevyStep(d, beta_L)                      Eq. (24)-(25)
         X_new[i] <- X[i] + gamma(LX)[i]                            Eq. (23),
           + beta_t (x_hub - X[i]) (*) Levy_i                       (30)
      else                                                          EXPLOITATION
         N(i) <- { j : A[i,j] > 0 }
         if N(i) != empty then
            eta_ij <- A[i,j] / sum_k A[i,k]                         Eq. (31)
            m_avg <- sum_j eta_ij (X[j]-X[i])                       Eq. (32)
            j* <- argmin_{j in N(i)} F[j]
            m_best <- X[j*] - X[i]                                  Eq. (33)
            X_new[i] <- X[i]+m_avg+0.5 m_best                       Eq. (34)
         else
            X_new[i] <- X[i]
         end
      end
```

```
    X_new[i] <- clip(X_new[i], lb, ub)                          Eq. (35)
  end
  F_new[i] <- f(X_new[i])  for i = 1..N
  improved <- (F_new < F)                                       Eq. (36)
  X[improved]<-X_new[improved]; F[improved]<-F_new[improved]
  p_s <- mean(improved)                                         Eq. (37)
  gamma <- clip(gamma*(1.05 if p_s>0.20 else 0.95),             Eq. (38)-
      gamma_min, gamma_max)                                     (39)
  if t mod 50 == 0 then                                         Sec. 3.13
    X_opp <- clip(lb + ub - X, lb, ub)                          Eq. (40)
    better <- f(X_opp) < F                                      Eq. (41)
    X[better] <- X_opp[better]
  end
  if mean(std(X, axis=0)) < 1e-4 then                           Eq. (42)
    worst <- indices of worst 80% agents by F                   Eq. (43)
    X[worst] <- Initialize(|worst|, d, lb, ub)
    F[worst] <- f(X[worst])
  end
  worst_idx <- indices of the n_elite largest F
  X[worst_idx]<-X_elite; F[worst_idx]<-F_elite                  restore elites
  if min(F)<F*: (x*,F*)<-(X[argmin F], min F)                   Eq. (45)
  Convergence_curve[t] <- F*
end
return x*, F*, Convergence_curve
```

3.18. Algorithmic Flowchart

Figure 6 illustrates the control flow of Algorithm 1, highlighting the branch between the exploration (Laplacian-diffusion / Lévy) and exploitation (neighbourhood message-passing) operators, and the three stabilization mechanisms — elitism, opposition-based learning, and diversity-triggered restart — that wrap the core update.

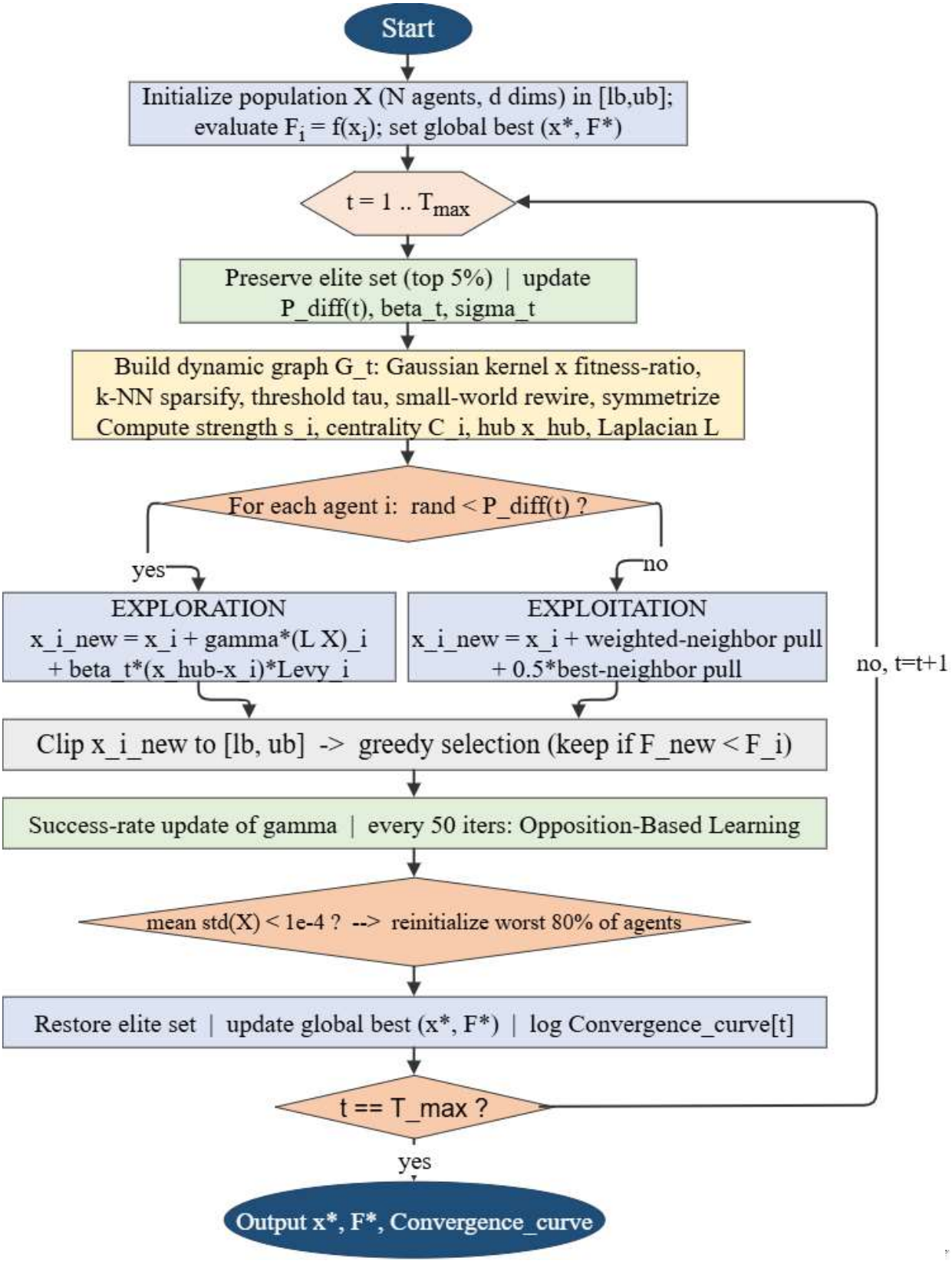


Figure 6. Flowchart of the Graph Dynamics Optimizer (GDO).

3.19. Computational Complexity

Per iteration, GDO evaluates the objective 2N times in the worst case (N population updates plus, on OBL iterations, N opposite-point evaluations), and constructs the pairwise distance/kernel matrices in $O(N^2d)$ time for the graph-building step; the k-NN restriction, Laplacian multiplication and centrality/degree computations are also $O(N^2d)$ and $O(N^2)$, respectively, dominating the O(Nd) cost of the update and selection steps. The overall per-run complexity is therefore $O(T \cdot N^2 \cdot d)$, the same order as other graph- or distance-matrix-based population metaheuristics.

4. Results and Discussion

4.1. Experimental setup and performance metrics

The performance of GDO-LDOL was tested on the R.T.C. France benchmark (Table 3) for three equivalent-circuit models with 9 (TDM), 10 (MTDM) and 11 (VVR-TDM) unknown parameters. All eight algorithms (GDO-LDOL, PSO, APO, ARO, DO, SMA, ZOA and DOA) were executed with the same population size and iteration budget (Table 2): 30 agents, 1000 iterations and 30 independent runs per model. The objective function was the RMSE between measured and model predicted current (Eq. (4)). minimum, maximum, mean, median, standard deviation and variance of the final RMSE over the 30 runs are reported for every algorithm. The minimum characterizes the achievable accuracy, while the mean, the standard deviation and the maximum characterize reliability in relation to a random initialization. Also for the best run of GDO-LDOL, the identified parameters, the point-wise current and power errors and the reconstructed I-V and P-V curves are shown. The parameter ranges searched are given in Tables 5, 8 and 11.

4.2. Triple Diode Model (TDM)

The statistical results summarized in Table 4 show that GDO-LDOL achieves the lowest minimum RMSE (7.42486×10^{-4}) among all eight competing algorithms, outperforming PSO (7.63772×10^{-4}), APO (7.76025×10^{-4}), ARO (7.85511×10^{-4}), and substantially outperforming DO, SMA, ZOA, and DOA, the latter of which converged to a markedly inferior minimum RMSE of 1.135075×10^{-3}. More importantly for practical applicability, GDO-LDOL also records the lowest mean RMSE (1.054126×10^{-3}) and the lowest standard deviation (2.43126×10^{-4}) across the 30 independent runs, indicating that its superior accuracy is not the result of a single favourable run but reflects consistent, repeatable performance. This is corroborated by the RMSE boxplot in Figure 9, where GDO-LDOL exhibits the most compact interquartile range and the lowest median among all algorithms, while DOA shows both a high median and a long upper tail with several extreme outliers, reflecting its susceptibility to premature convergence on this model.

The convergence behaviour illustrated in Figure 10 further supports this observation: GDO-LDOL descends rapidly within the first ~100–150 iterations and stabilizes near its final RMSE well before the 1000-iteration budget is exhausted, whereas SMA and DOA continue to exhibit stepwise improvements late into the run, indicative of a less efficient exploration–exploitation balance. The best-run parameter estimates reported in Table 5 are physically consistent with the R.T.C. France cell specifications (Table 1): the estimated photocurrent (Iph ≈ 0.7608 A) closely matches the datasheet short-circuit current (Isc = 0.7605 A), and the ideality factors n1, n2, n3 remain within the physically admissible range [1, 2]. The close agreement between the experimental and GDO-LDOL-predicted I–V and P–V curves (Figures 7 and 8) — with absolute current errors not exceeding ~1.36 mA across the full voltage range (Table 6) — confirms the model's ability to capture both the linear and exponential regions of the characteristic curve, including the knee region near the maximum power point. The current and power error distributions (Figures 11 and 12) show that the largest deviations for all algorithms occur near the open-circuit voltage region, where the sharp exponential rise makes the fitting problem locally ill-conditioned; nonetheless, GDO-LDOL's errors in this region remain comparable to or smaller than those of the next-best algorithms.

Table 4. Best RMSE Metrics of the Optimization Algorithms over 30 Runs (TDM)

Metric	GDO-LDOL	PSO	APO	ARO	DO	SMA	ZOA	DOA
Min	0.000742486	0.000763772	0.000776025	0.000785511	0.000839179	0.000861564	0.000872747	0.001135075
Max	0.001536173	0.002083251	0.002474117	0.002086578	0.004360139	0.00613579	0.003887539	0.024135818
Mean	0.001054126	0.001306833	0.00130069	0.0013171	0.001963999	0.002149267	0.002155133	0.005993514
Median	0.001031532	0.001288135	0.0011878	0.001271666	0.001829183	0.001927503	0.002101497	0.002910283
Std Dev	0.000243126	0.000399056	0.000410581	0.000344989	0.000797537	0.001084426	0.000774026	0.007182684
VAR.	5.91E-08	1.592E-07	1.686E-07	0.000000119	6.361E-07	0.000001176	5.991E-07	5.15909E-05

Table 5. The TDM parameter identification Obtained by Optimization Algorithms (Best Run)

Par.	LB	UB	GDO-LDOL	PSO	APO	ARO	DO	SMA	ZOA	DOA
Iph (A)	0	1	0.76082791	0.76078144	0.76089759	0.76058383	0.76034719	0.76097157	0.76139431	0.76155342
Isd1(A)	0	1e-6	1.036952e-07	2.553010e-07	2.477327e-07	2.508224e-10	7.306864e-07	3.015545e-08	4.187022e-07	6.517777e-07
Isd2(A)	0	1e-6	4.320015e-08	3.858414e-07	1.498408e-07	2.137489e-07	3.832398e-08	1.567455e-07	1.948631e-07	5.013625e-08
Isd3(A)	0	1e-6	1.000000e-06	0.000000e+00	3.191938e-08	2.754696e-07	4.975068e-14	2.192819e-07	1.191752e-07	5.666424e-07
Rs(Ω)	0	0.5	0.03754343	0.03662433	0.03699852	0.03635414	0.03818689	0.03769197	0.03752677	0.03566741
Rsh(Ω	0	100	55.386445	54.551467	51.305655	57.185466	63.356646	47.056786	45.718866	61.380751
n1	1.0	2.0	1.39146584	1.46146337	1.45762304	1.38496442	1.69245471	1.94587087	1.76601133	1.98463913
n2	1.0	2.0	1.64120907	1.94082729	1.86450809	1.81560143	1.32852131	1.98001445	1.85722609	1.36693081
n3	1.0	2.0	1.8744602	2	1.85545679	1.46994233	1.05688766	1.44461023	1.40181908	1.63992366

Table 6. Experimental vs. predicted current of GDO-LDOL for TDM (Best run).

#	V (V)	I_exp (A)	I_pred (A)	Abs Error (A)	Error %	P_exp (W)	P_pred (W)	P Error (W)
1	-0.2057	0.764	0.76402504	2.50378E-05	0.003277	-0.1571548	-0.15715995	5.1503E-06
2	-0.1291	0.762	0.76264285	0.000642852	0.084364	-0.0983742	-0.09845719	8.29922E-05
3	-0.0588	0.7605	0.76137398	0.000873981	0.114922	-0.0447174	-0.04476879	5.13901E-05
4	0.0057	0.7605	0.76020848	0.000291521	0.038333	0.00433485	0.00433319	1.6617E-06
5	0.0646	0.76	0.75913987	0.000860128	0.113175	0.049096	0.04904044	5.55643E-05
6	0.1185	0.759	0.75814914	0.000850863	0.112103	0.0899415	0.08984067	0.000100827
7	0.1678	0.757	0.75720753	0.000207525	0.027414	0.1270246	0.12705942	3.48228E-05
8	0.2132	0.757	0.75624852	0.000751477	0.09927	0.1613924	0.16123219	0.000160215
9	0.2545	0.7555	0.75515752	0.000342482	0.045332	0.19227475	0.19218759	8.71617E-05
10	0.2924	0.754	0.75366725	0.000332746	0.044131	0.2204696	0.22037231	9.72948E-05
11	0.3269	0.7505	0.75129851	0.000798511	0.106397	0.24533845	0.24559948	0.000261033
12	0.3585	0.7465	0.74716233	0.000662329	0.088725	0.26762025	0.2678577	0.000237445
13	0.3873	0.7385	0.73984748	0.001347481	0.182462	0.28602105	0.28654293	0.000521879
14	0.4137	0.728	0.72715754	0.000842458	0.115722	0.3011736	0.30082508	0.000348525
15	0.4373	0.7065	0.70681506	0.000315055	0.044594	0.30895245	0.30909022	0.000137774
16	0.459	0.6755	0.67532521	0.00017479	0.025876	0.3100545	0.30997427	8.02288E-05
17	0.4784	0.632	0.63107793	0.000922071	0.145897	0.3023488	0.30190768	0.000441119
18	0.496	0.573	0.57236025	0.000639746	0.111648	0.284208	0.28389069	0.000317314
19	0.5119	0.499	0.49973699	0.000736987	0.147693	0.2554381	0.25581536	0.000377264
20	0.5265	0.413	0.41360479	0.000604792	0.146439	0.2174445	0.21776292	0.000318423
21	0.5398	0.3165	0.31715511	0.000655115	0.206987	0.1708467	0.17120033	0.000353631
22	0.5521	0.212	0.21189188	0.000108116	0.050998	0.1170452	0.11698551	5.96909E-05
23	0.5633	0.1035	0.10245487	0.001045133	1.00979	0.05830155	0.05771283	0.000588723
24	0.5736	-0.01	-0.00944315	0.000556845	5.568454	-0.005736	-0.00541659	0.000319407
25	0.5833	-0.123	-0.12435505	0.001355046	1.101664	-0.0717459	-0.0725363	0.000790398
26	0.59	-0.21	-0.20890832	0.001091682	0.519848	-0.1239	-0.12325591	0.000644092

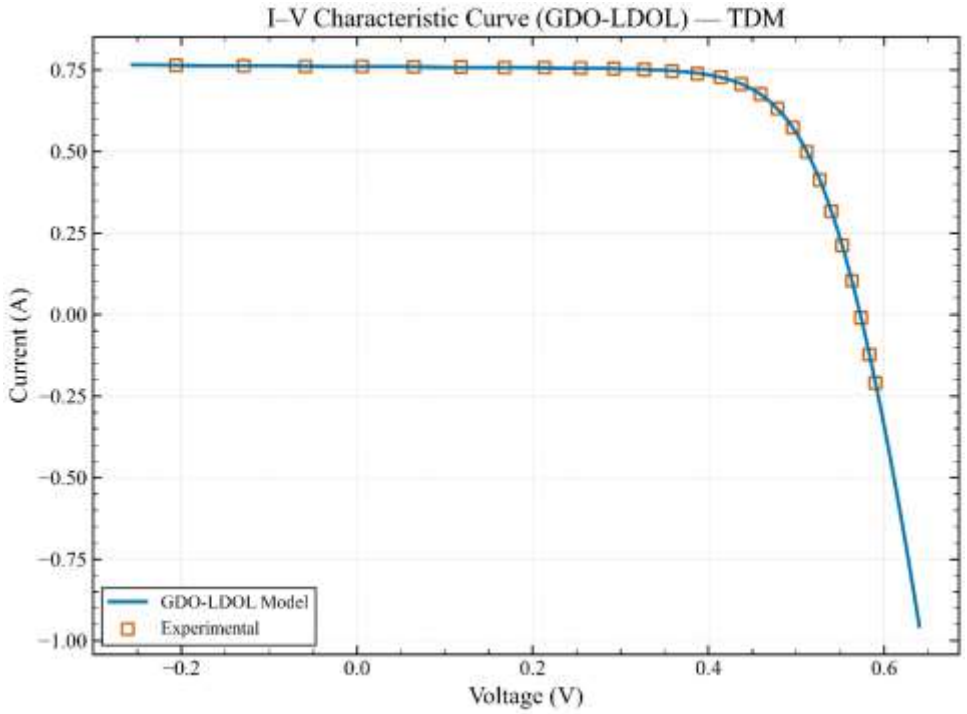


Figure 7. I–V Characteristics of the TDM for the GDO-LDOL (Best Run)

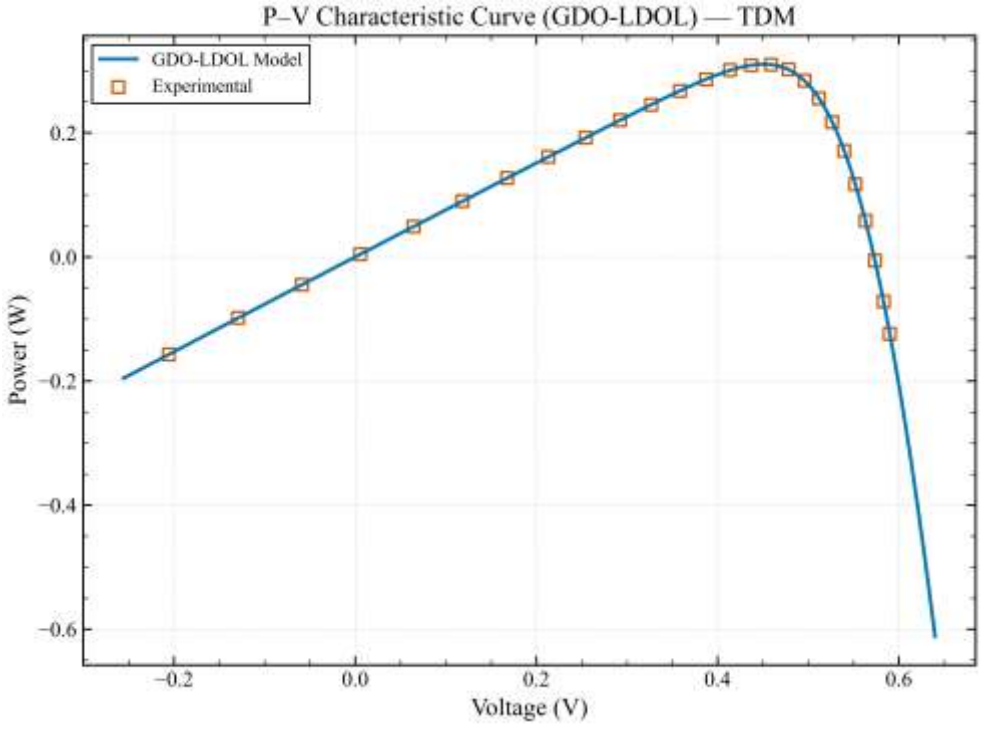


Figure 8. P–V Characteristics of the TDM for the GDO-LDOL (Best Run)

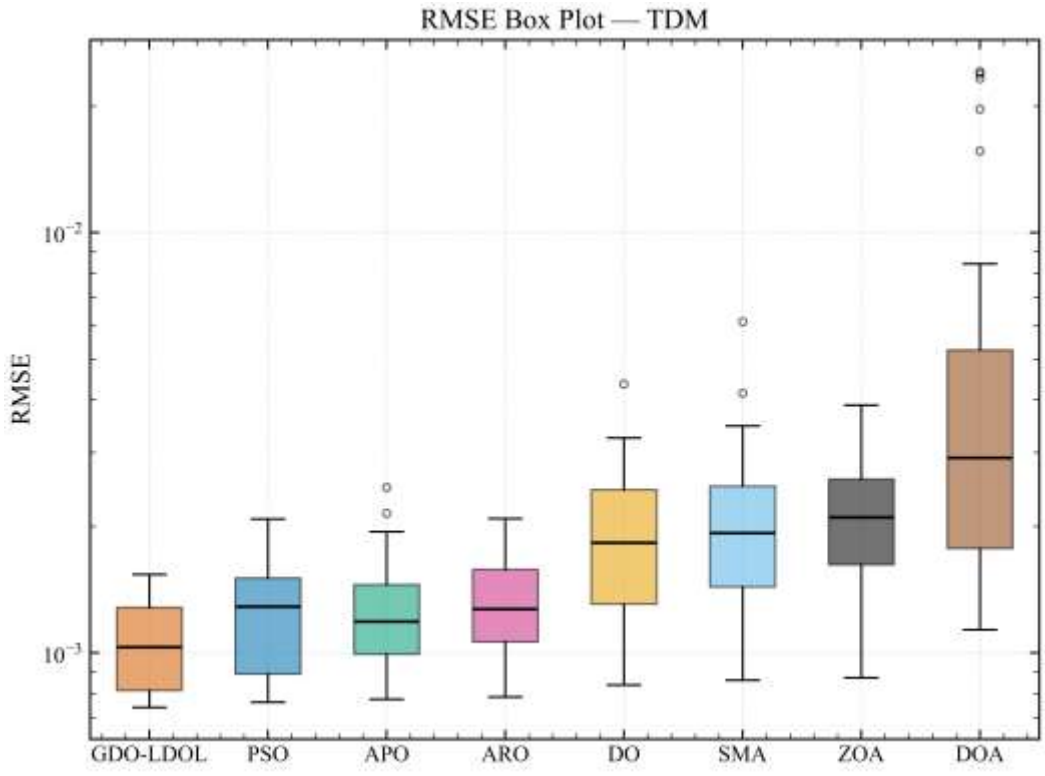


Figure 9. RMSE Boxplot of Optimization Algorithms for TDM (30 Runs).

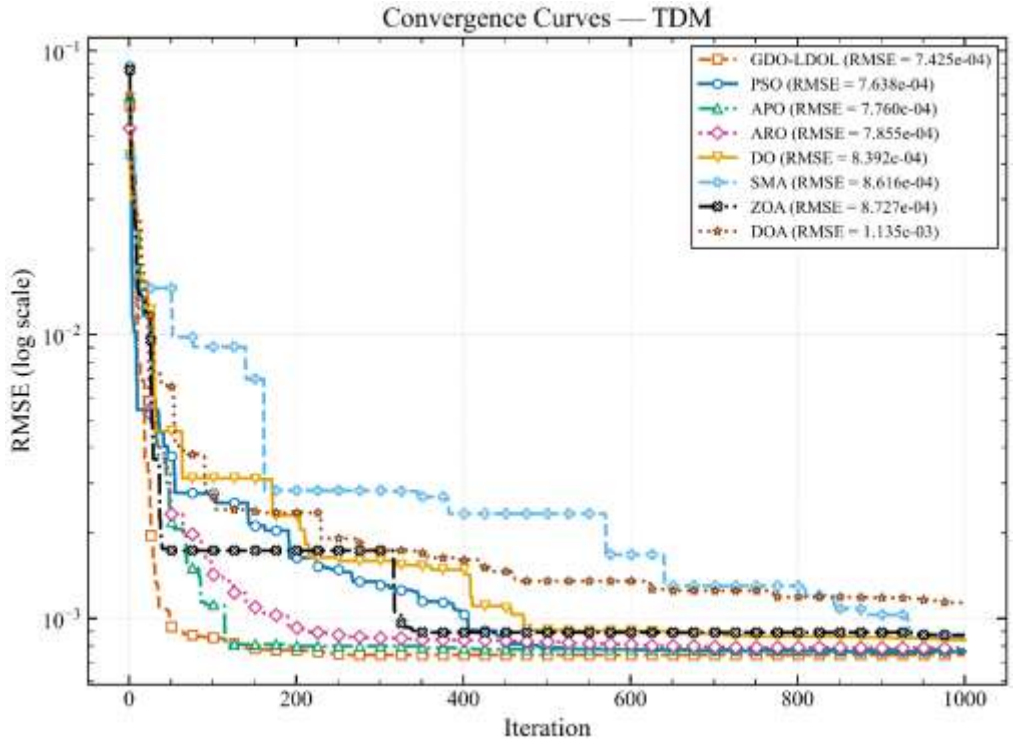


Figure 10. Convergence Curve for TDM via Optimization Algorithms (Best Run)

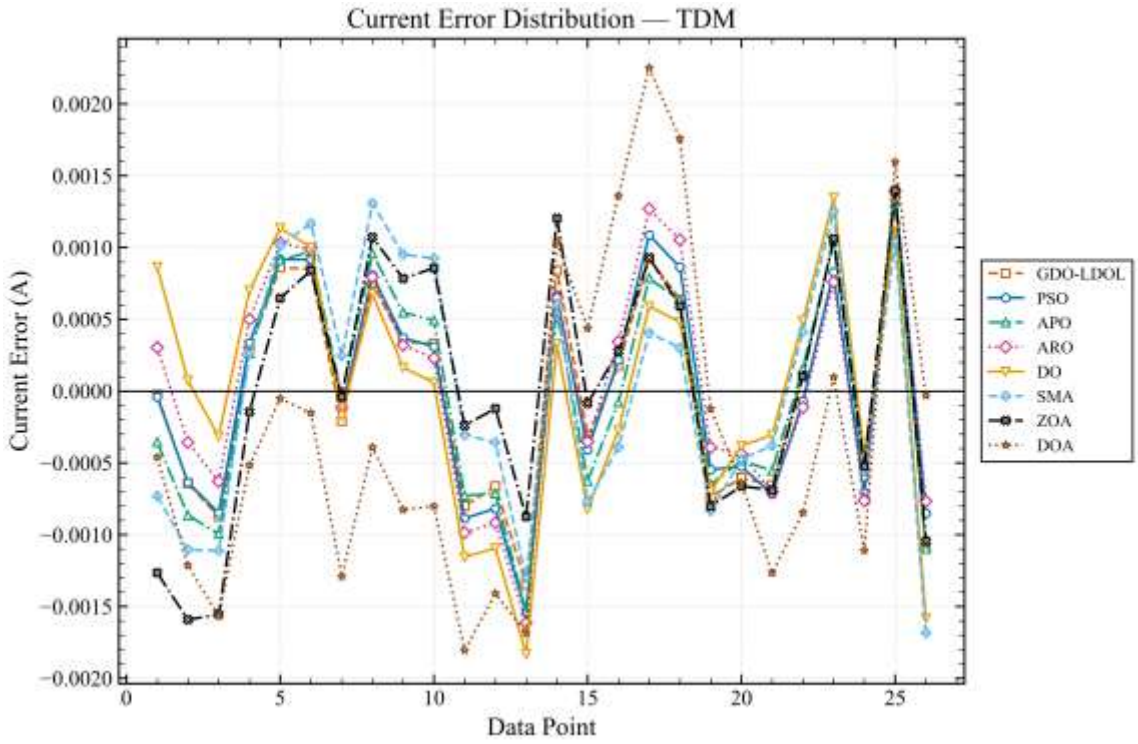


Figure 11. Current Error Distribution of Optimization Algorithms for TDM.

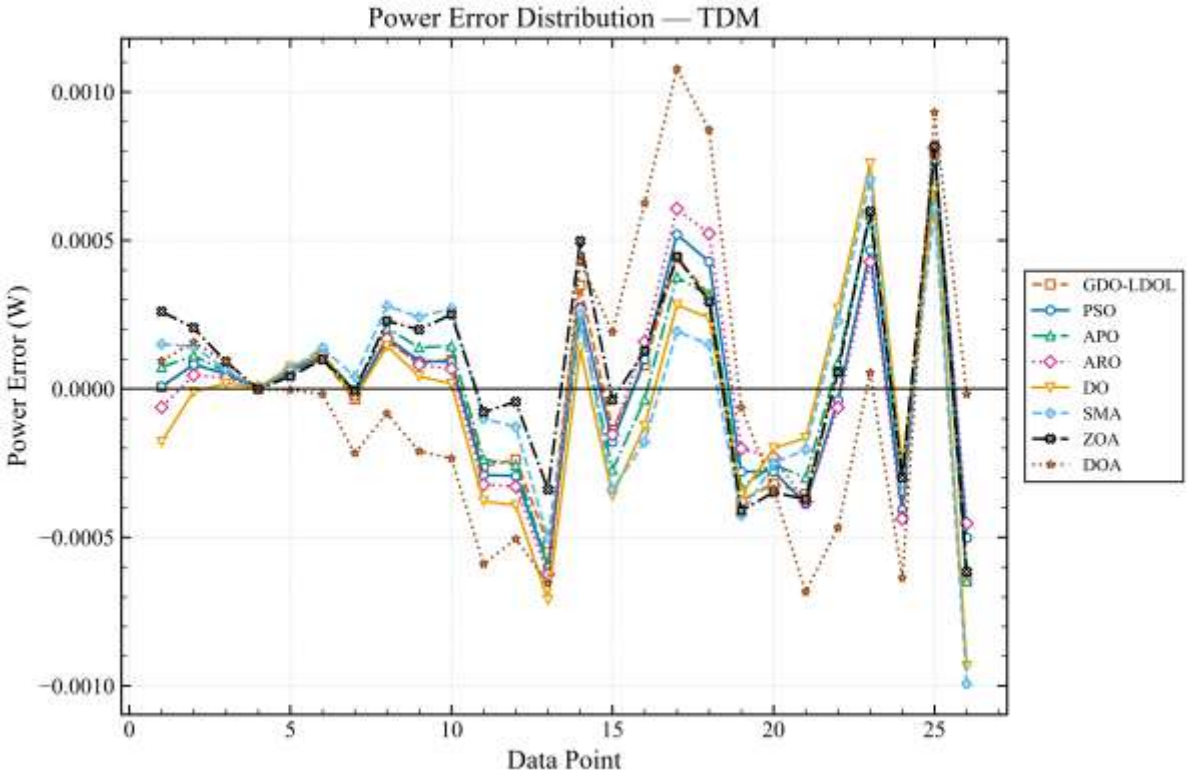


Figure 12. Power Error Distribution of Optimization Algorithms for TDM.

4.3. Modified Triple Diode Model (MTDM)

The introduction of the additional series resistance term (Rm) in the MTDM increases the parameter space to ten decision variables, raising the dimensionality and nonlinearity of the estimation problem. Despite this added complexity, Table 7 shows that GDO-LDOL maintains its lead, achieving the lowest minimum RMSE (7.40549×10^{-4}), statistically indistinguishable from ARO's minimum (7.40557×10^{-4}), but with a substantially better mean RMSE (1.043911×10^{-3} versus ARO's 1.135176×10^{-3}, an improvement of approximately 8%) and a comparable standard deviation. The contrast with PSO is particularly notable: while PSO's minimum RMSE (7.46515×10^{-4}) is competitive, its maximum RMSE across 30 runs balloons to 1.54389×10^{-2}, nearly two orders of magnitude worse than its best run, and its standard deviation (2.587485×10^{-3}) is an order of magnitude larger than GDO-LDOL's. This instability is visually confirmed in the RMSE boxplot (Figure 15), where PSO displays multiple high-RMSE outliers, indicating that classical leader-following swarm dynamics can occasionally become trapped in poor local optima when the search space grows more rugged — a failure mode that GDO-LDOL's graph-based hub attraction and stagnation-triggered diversity restarts are specifically designed to mitigate.

The convergence curves in Figure 16 show GDO-LDOL and ARO converging fastest and to the lowest asymptotic RMSE, both stabilizing within the first 200 iterations, while DO, SMA, ZOA, and DOA continue to make incremental gains throughout the run without closing the gap. The estimated parameters (Table 8) again lie within physically meaningful bounds, and the additional series-resistance term Rm converges to a small but non-trivial value (≈0.223 Ω for GDO-LDOL), consistent with its intended role of modelling localized resistive effects in the third diode branch. The I–V and P–V fits (Figures 13 and 14) and the corresponding error table (Table 9) show absolute current errors remaining below ~1.36 mA across the dataset, with the largest percentage errors again concentrated near the low-current, near-open-circuit points (points 23–26), where the experimental current approaches zero and small absolute errors translate into large relative errors — a well-known artefact of RMSE-based fitting rather than a deficiency specific to any one algorithm.

Table 7. Best RMSE Metrics of the Optimization Algorithms over 30 Runs (MTDM)

Metric	GDO-LDOL	PSO	APO	ARO	DO	SMA	ZOA	DOA
Min	0.000740549	0.000746515	0.000771858	0.000740557	0.000809067	0.000822031	0.000759189	0.001047196
Max	0.001717439	0.015438931	0.002595058	0.001971848	0.003799224	0.006062655	0.004550924	0.025127251
Mean	0.001043911	0.001766151	0.001397285	0.001135176	0.002160755	0.002240594	0.002202039	0.006287923
Median	0.000942482	0.001223269	0.001298961	0.001110565	0.002056143	0.001997738	0.002014102	0.003132406
Std Dev	0.000254355	0.002587485	0.000519466	0.00031973	0.000790352	0.001071058	0.000950225	0.006609094
VAR.	6.47E-08	6.6951E-06	2.698E-07	1.022E-07	6.247E-07	1.1472E-06	9.029E-07	4.36801E-05

Table 8. The MTDM parameter identification Obtained by Optimization Algorithms (Best Run)

Par.	LB	UB	GDO-LDOL	PSO	APO	ARO	DO	SMA	ZOA	DOA
Iph (A)	0	1	0.7607731	0.76079999	0.76075071	0.76083717	0.76050943	0.76078653	0.76094928	0.76093594
Isd1(A)	0	1e-6	1.090490e-07	9.902064e-08	2.496125e-07	3.951501e-07	3.473077e-07	1.088668e-12	5.027389e-07	3.065141e-07
Isd2(A)	0	1e-6	2.877099e-07	3.357724e-07	2.120877e-07	7.594875e-08	1.303031e-07	3.705924e-07	1.843502e-07	1.622944e-07
Isd3(A)	0	1e-6	9.999479e-07	5.135957e-07	1.031966e-07	9.675341e-07	3.600079e-08	6.089332e-10	3.430921e-07	2.495074e-07
Rs(Ω)	0	0.5	0.0375402	0.03738263	0.03638559	0.03799792	0.03654392	0.03577696	0.03722344	0.03876255
Rsh(Ω	0	100	56.550982	55.328712	55.22682	55.862611	55.848741	56.212653	52.237992	52.145239
n1	1.0	2.0	1.38882236	1.39136597	1.46046925	1.88186095	1.81168235	1.06754236	1.9778581	1.99942949
n2	1.0	2.0	1.9957959	2	1.93320304	1.36047206	1.40985127	1.49550549	1.43281226	1.41853652
n3	1.0	2.0	1.9113901	1.73341425	1.74809758	1.89626311	1.45782636	1.4648945	1.97290225	1.96805736
Rsm(Ω)	0	0.5	0.22267599	0.00074032	0.46430526	0.28901414	0.37265335	0.00020815	0.28785665	0.14204638

Table 9. Experimental vs. predicted current of GDO-LDOL for MTDM (Best run).

#	V (V)	I_exp (A)	I_pred (A)	Abs Error (A)	Error %	P_exp (W)	P_pred (W)	P Error (W)
1	-0.2057	0.764	0.76390478	9.52161E-05	0.0125	-0.1571548	-0.15713521	1.9586E-05
2	-0.1291	0.762	0.76255101	0.000551007	0.0723	-0.0983742	-0.09844534	7.1135E-05
3	-0.0588	0.7605	0.76130813	0.000808133	0.1063	-0.0447174	-0.04476492	4.7518E-05
4	0.0057	0.7605	0.76016629	0.000333714	0.0439	0.00433485	0.00433295	1.9022E-06
5	0.0646	0.76	0.75911884	0.000881161	0.1159	0.049096	0.04903908	5.6923E-05
6	0.1185	0.759	0.75814662	0.000853377	0.1124	0.0899415	0.08984037	0.00010113
7	0.1678	0.757	0.75722059	0.000220591	0.0291	0.1270246	0.12706162	3.7015E-05
8	0.2132	0.757	0.75627412	0.000725878	0.0959	0.1613924	0.16123764	0.00015476
9	0.2545	0.7555	0.75519268	0.000307316	0.0407	0.19227475	0.19219654	7.8212E-05
10	0.2924	0.754	0.75371	0.000290004	0.0385	0.2204696	0.2203848	8.4797E-05
11	0.3269	0.7505	0.75134798	0.000847977	0.113	0.24533845	0.24561565	0.0002772
12	0.3585	0.7465	0.74721808	0.000718079	0.0962	0.26762025	0.26787768	0.00025743
13	0.3873	0.7385	0.73990702	0.001407017	0.1905	0.28602105	0.28656599	0.00054494

14	0.4137	0.728	0.72721357	0.000786434	0.108	0.3011736	0.30084825	0.00032535
15	0.4373	0.7065	0.70685586	0.00035586	0.0504	0.30895245	0.30910807	0.00015562
16	0.459	0.6755	0.6753394	0.000160597	0.0238	0.3100545	0.30998079	7.3714E-05
17	0.4784	0.632	0.63106347	0.000936525	0.1482	0.3023488	0.30190077	0.00044803
18	0.496	0.573	0.57232701	0.000672986	0.1175	0.284208	0.2838742	0.0003338
19	0.5119	0.499	0.49970243	0.000702435	0.1408	0.2554381	0.25579768	0.00035958
20	0.5265	0.413	0.41358498	0.000584976	0.1416	0.2174445	0.21775249	0.00030799
21	0.5398	0.3165	0.31715749	0.00065749	0.2077	0.1708467	0.17120161	0.00035491
22	0.5521	0.212	0.21191363	8.63706E-05	0.0407	0.1170452	0.11699751	4.7685E-05
23	0.5633	0.1035	0.1024845	0.001015497	0.9812	0.05830155	0.05772952	0.00057203
24	0.5736	-0.01	-0.00942142	0.000578581	5.7858	-0.005736	-0.00540413	0.00033187
25	0.5833	-0.123	-0.12435888	0.001358877	1.1048	-0.0717459	-0.07253853	0.00079263
26	0.59	-0.21	-0.20894187	0.001058125	0.5039	-0.1239	-0.12327571	0.00062429

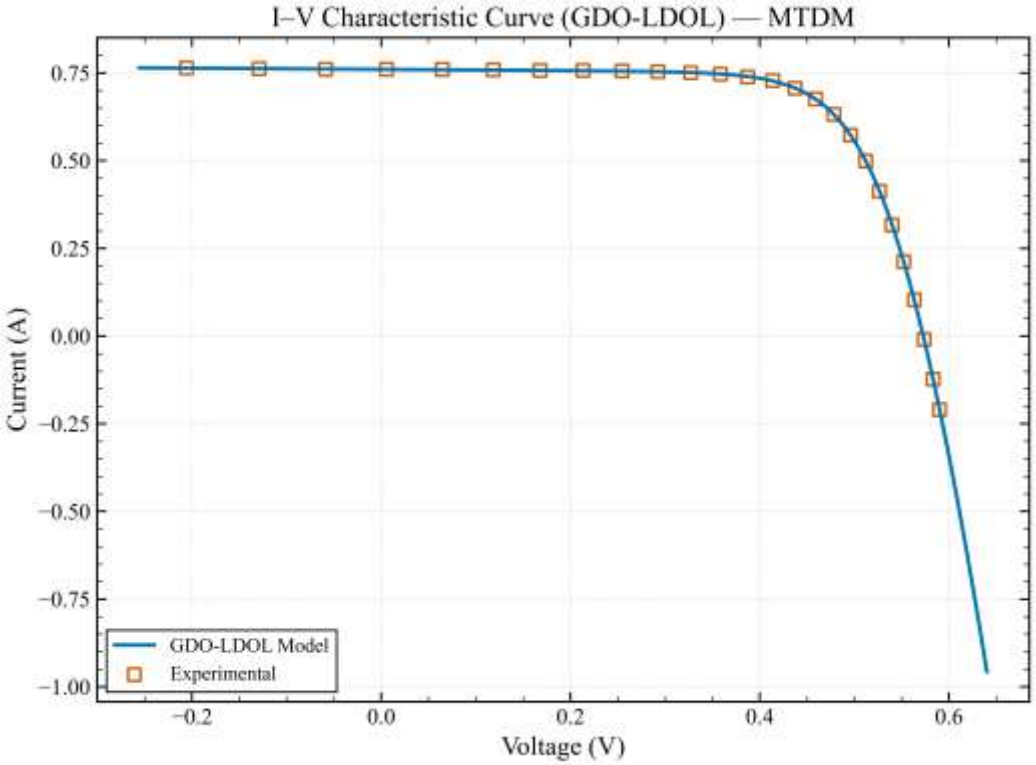


Figure 13. I–V Characteristics of the MTDM for the GDO-LDOL (Best Run)

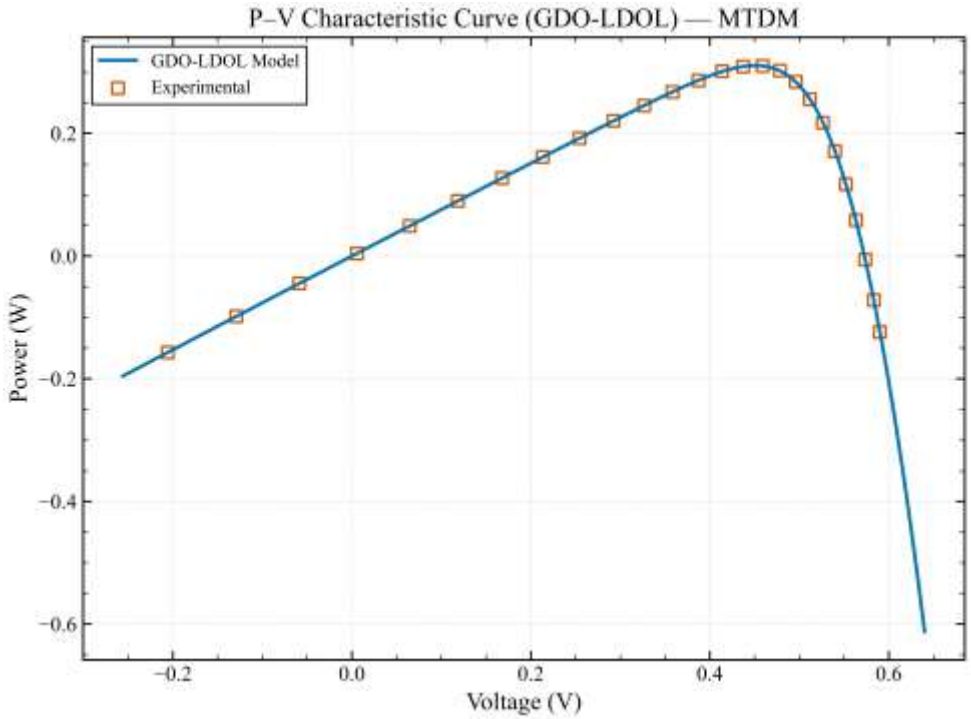


Figure 14. P–V Characteristics of the MTDM for GDO-LDOL (Best Run)

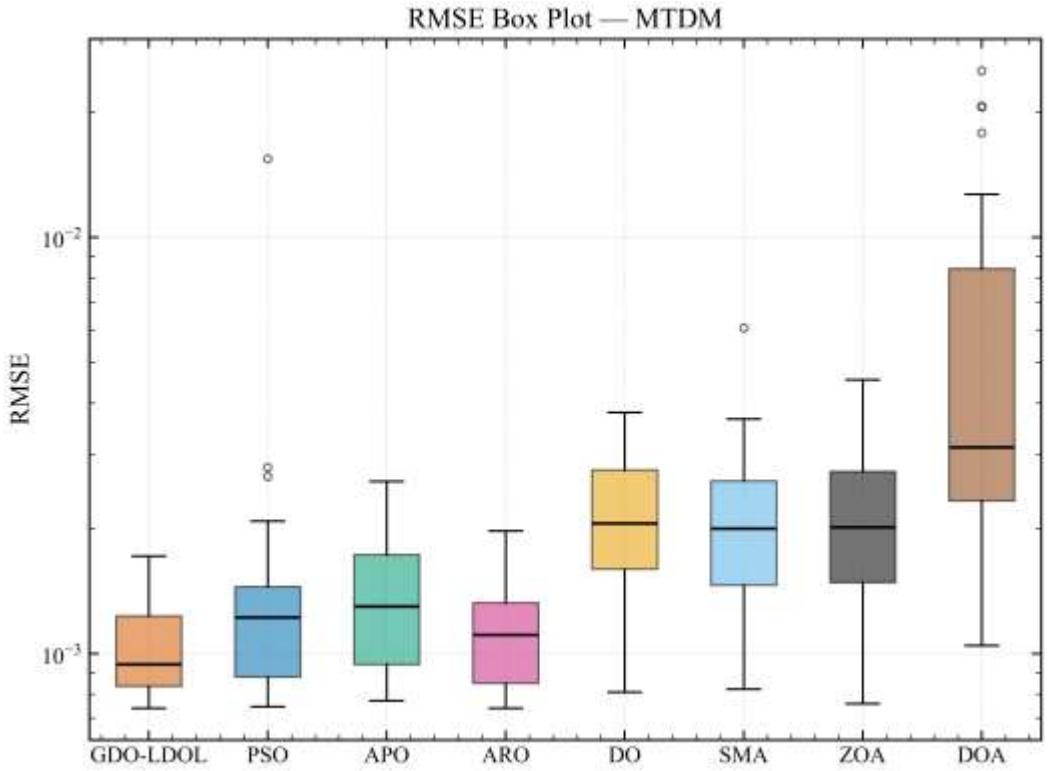


Figure 15. RMSE Boxplot of Optimization Algorithms for MTDM (30 Runs).

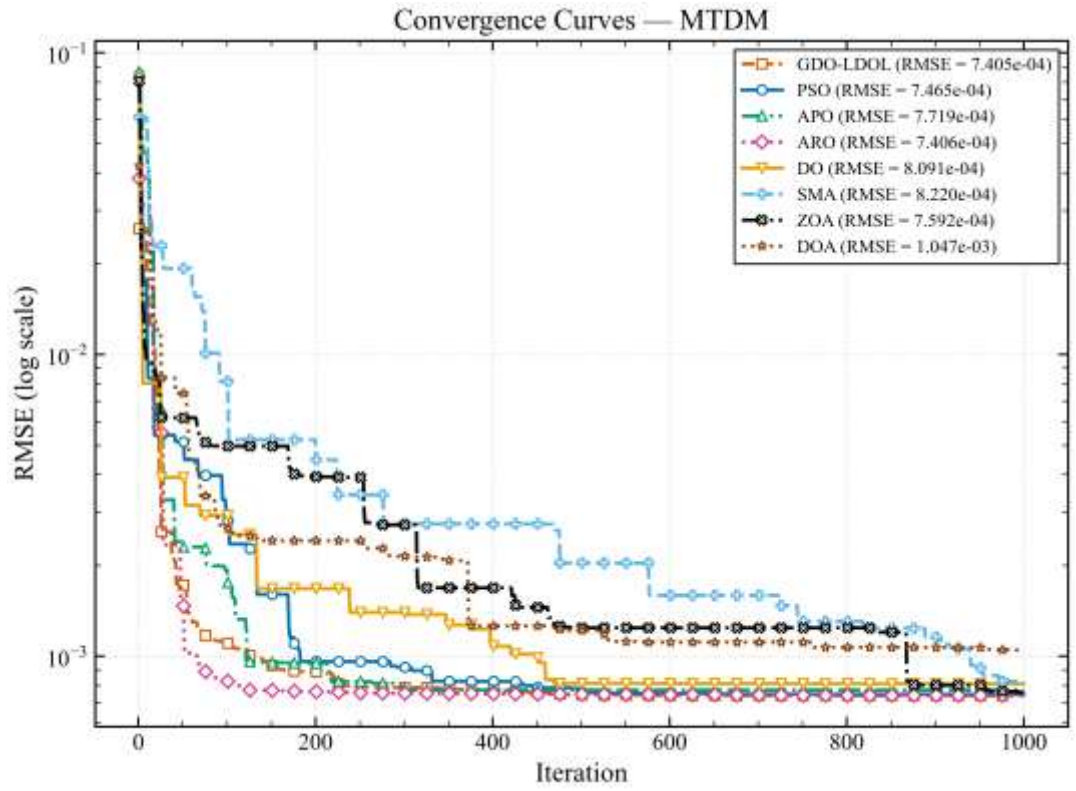


Figure 16. Convergence Curve for MTDM via Optimization Algorithms (Best Run).

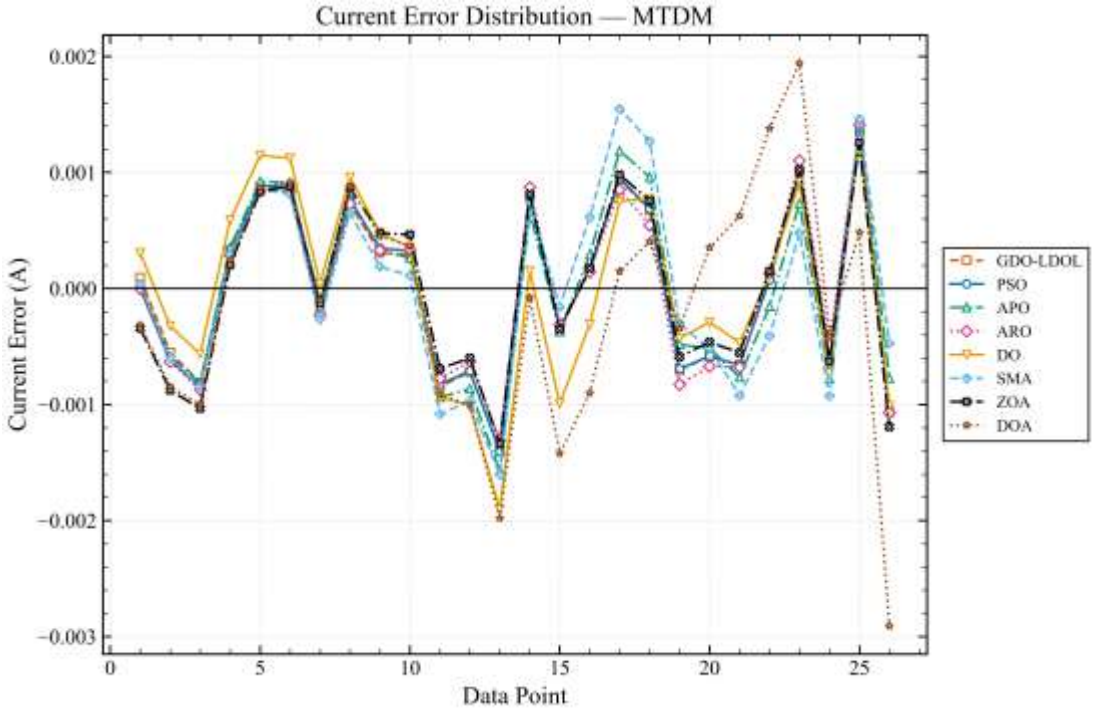


Figure 17. Current Error Distribution of Optimization Algorithms for MTDM.

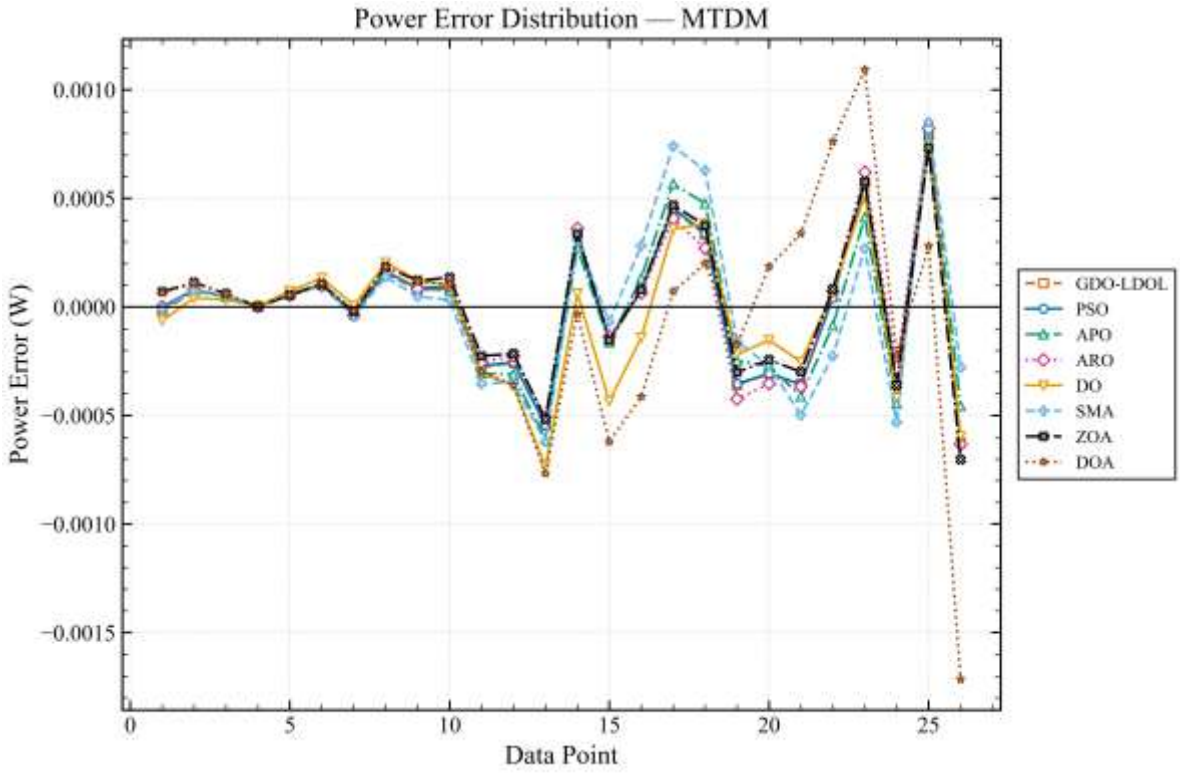


Figure 18. Power Error Distribution of Optimization Algorithms for MTDM.

4.4. VVR - Triple Diode Model (VVR- TDM)

The VVR-TDM, which replaces the fixed series and shunt resistances with voltage-dependent terms (Rso, Rpo, Ks, Kp), represents the most physically detailed and numerically demanding of the three models. Table 10 shows that GDO-LDOL achieves the lowest minimum RMSE overall across all three models and all eight algorithms (7.25153×10^{-4}), and — critically — the lowest mean RMSE (7.62391×10^{-4}) with an exceptionally small standard deviation (2.68447×10^{-5}), second only to APO (2.05956×10^{-5}). This places GDO-LDOL and APO as the two most stable algorithms for this model, both markedly outperforming PSO, DO, SMA, ZOA, and DOA in terms of run-to-run consistency. Notably, several algorithms that performed competitively on the simpler TDM and MTDM formulations — including PSO, DO, SMA, ZOA, and DOA — exhibit sharp degradation on VVR-TDM, with maximum RMSE values reaching into the 10^{-2} range (e.g., ZOA's maximum of 1.1101×10^{-2}) despite having near-identical minimum RMSE to GDO-LDOL. This divergence between best-case and worst-case performance, visible in the wide boxes and long whiskers of Figure 21, underscores that the VVR-TDM's voltage-coupled resistance terms introduce additional local optima that expose weaknesses in exploration strategies not apparent in the simpler models.

The convergence curves for VVR-TDM (Figure 22) show a distinctive pattern relative to TDM and MTDM: nearly all algorithms exhibit a very sharp initial drop within the first ~50 iterations, after which GDO-LDOL, PSO, APO, and ARO converge to a tight cluster near the global optimum, while ZOA and SMA plateau at a visibly higher RMSE. This suggests that the VVR-TDM's landscape, despite its added parameters, has a strong initial gradient toward a broad basin of attraction, but only algorithms with an effective refinement mechanism — such as GDO-LDOL's neighbourhood message-passing exploitation operator — can fully exploit it. The best-run parameters (Table 11) show physically reasonable values for the voltage-coefficients Ks ($\approx -7.3\times10^{-4}$) and Kp ($\approx -0.047$), consistent with a mild voltage-dependence of the series and shunt resistances. The I–V and P–V agreement (Figures 19 and 20) is visually indistinguishable from the experimental data across the entire operating range, and the error table (Table 12) confirms sub-millampere absolute current errors throughout, including in the previously problematic near-Voc region.

Table 10. Best RMSE Metrics of the Optimization Algorithms over 30 Runs (VVR-TDM)

Metric	GDO-LDOL	PSO	APO	ARO	DO	SMA	ZOA	DOA
Min	0.000725153	0.000732274	0.000740694	0.000732298	0.000730526	0.000754789	0.000755949	0.000762959
Max	0.000851978	0.008498215	0.000821261	0.001176167	0.008502736	0.008665269	0.011101133	0.005286221
Mean	0.000762391	0.001064308	0.000770598	0.000806045	0.001550731	0.003146652	0.002894359	0.001670094
Median	0.000753057	0.000814493	0.000766021	0.000780165	0.000822008	0.000937626	0.001025289	0.000976968
Std Dev	2.68447E-05	0.001381272	2.05956E-05	9.97235E-05	0.001842553	0.003213723	0.003302812	0.00127698
VAR.	7E-10	1.9079E-06	4E-10	9.9E-09	0.000003395	0.000010328	1.09086E-05	1.6307E-06

Table 11. The VVR-TDM parameter identification using Optimization Algorithms (Best Run)

Par.	LB	UB	GDO-LDOL	PSO	APO	ARO	DO	SMA	ZOA	DOA
Iph (A)	0.7608	0.7609	0.7608	0.76082112	0.76088476	0.76083946	0.7609	0.7608	0.7608	0.76089447
Isd1(A)	1.00e-08	1.00e-07	1E-07	1.000000e-07	9.556639e-08	9.843173e-08	9.116843e-08	9.467872e-08	8.040270e-08	9.790132e-08
Isd2(A)	1.00e-13	1.00e-11	1E-13	1.264071e-13	2.574647e-12	2.812461e-12	2.987146e-12	1.189881e-13	5.535696e-12	6.271038e-12
Isd3(A)	1.00e-05	1.00e-04	1E-05	3.033668e-05	2.997052e-05	2.496832e-05	1.034275e-05	2.584699e-05	2.291264e-05	8.009948e-05
n1	1.0	2.0	1.378566663	1.37683413	1.37296623	1.37570952	1.37092561	1.37243548	1.3598247	1.37363797
n2	1.0	4.0	1	4	1.90674368	1.78551777	1.50502674	3.85342464	3.67151578	1.21400897
n3	1.0	5.5	2.492247688	2.93902601	2.93373835	2.85149092	2.48658648	2.85516889	2.73902317	3.51265043
Rpo	60	75	64.78137915	67.559538	71.356591	67.326818	64.017788	74.774951	73.701121	74.89897

Par.	LB	UB	GDO-LDOL	PSO	APO	ARO	DO	SMA	ZOA	DOA
Rso	0.0035	0.04	0.03852797	0.03881127	0.03891293	0.03881561	0.03868197	0.03894103	0.03898236	0.03929131
Ks	-0.001	0.0001	-0.001	-0.001	-0.00073089	-0.00099743	-0.00088537	0.00009995	-0.00056052	0.00007069
Kp	-0.2	0.25	-0.047300767	0.25	-0.02204476	0.13587115	-0.08384468	0.01255563	0.05628049	0.24992908

Table 12. Experimental vs. predicted current of GDO-LDOL for VVR-TDM (Best run).

	V (V)	I_exp (A)	I_pred (A)	Abs Error (A)	Error %	P_exp (W)	P_pred (W)	P Error (W)
1	-0.2057	0.764	0.76350431	0.00049569	0.064881	-0.1571548	-0.15705284	0.000101963
2	-0.1291	0.762	0.76233796	0.000337962	0.044352	-0.0983742	-0.09841783	4.36309E-05
3	-0.0588	0.7605	0.7612573	0.000757299	0.099579	-0.0447174	-0.04476193	4.45292E-05
4	0.0057	0.7605	0.76025253	0.000247471	0.032541	0.00433485	0.00433344	1.4106E-06
5	0.0646	0.76	0.7593139	0.000686104	0.090277	0.049096	0.04905168	4.43223E-05
6	0.1185	0.759	0.75841665	0.000583353	0.076858	0.0899415	0.08987237	6.91273E-05
7	0.1678	0.757	0.75752254	0.000522539	0.069028	0.1270246	0.12711228	0.000087682
8	0.2132	0.757	0.75655398	0.000446019	0.058919	0.1613924	0.16129731	9.50913E-05
9	0.2545	0.7555	0.75538871	0.000111287	0.01473	0.19227475	0.19224643	2.83225E-05
10	0.2924	0.754	0.7537618	0.000238205	0.031592	0.2204696	0.22039995	6.96511E-05
11	0.3269	0.7505	0.75121587	0.000715867	0.095385	0.24533845	0.24557247	0.000234017
12	0.3585	0.7465	0.74690337	0.000403368	0.054034	0.26762025	0.26776486	0.000144607
13	0.3873	0.7385	0.73947179	0.00097179	0.13159	0.28602105	0.28639742	0.000376374
14	0.4137	0.728	0.72677825	0.001221748	0.167823	0.3011736	0.30066816	0.000505437
15	0.4373	0.7065	0.70656106	6.10599E-05	0.008643	0.30895245	0.30897915	2.67015E-05
16	0.459	0.6755	0.67528688	0.000213117	0.03155	0.3100545	0.30995668	9.78208E-05
17	0.4784	0.632	0.63125014	0.000749864	0.118649	0.3023488	0.30199007	0.000358735
18	0.496	0.573	0.5726491	0.000350899	0.061239	0.284208	0.28403395	0.000174046
19	0.5119	0.499	0.50000609	0.001006093	0.201622	0.2554381	0.25595312	0.000515019
20	0.5265	0.413	0.41373991	0.00073991	0.179155	0.2174445	0.21783406	0.000389563
21	0.5398	0.3165	0.31710993	0.000609926	0.19271	0.1708467	0.17117594	0.000329238
22	0.5521	0.212	0.21169539	0.000304611	0.143684	0.1170452	0.11687702	0.000168176
23	0.5633	0.1035	0.10219982	0.001300184	1.256216	0.05830155	0.05756916	0.000732394
24	0.5736	-0.01	-0.0096307	0.000369299	3.692987	-0.005736	-0.00552417	0.00021183
25	0.5833	-0.123	-0.12433152	0.001331522	1.082538	-0.0717459	-0.07252258	0.000776677
26	0.59	-0.21	-0.20863835	0.001361655	0.648407	-0.1239	-0.12309662	0.000803376

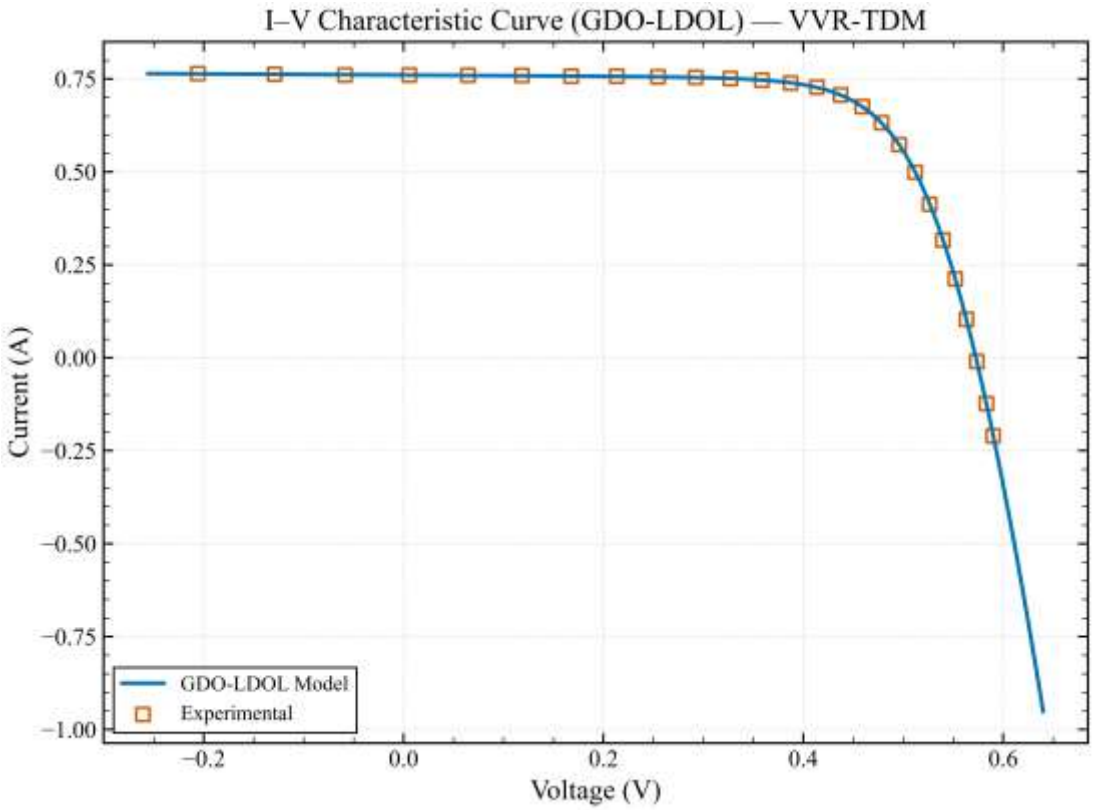


Figure 19. I–V Characteristics of the VVR-TDM for the GDO-LDOL (Best Run)

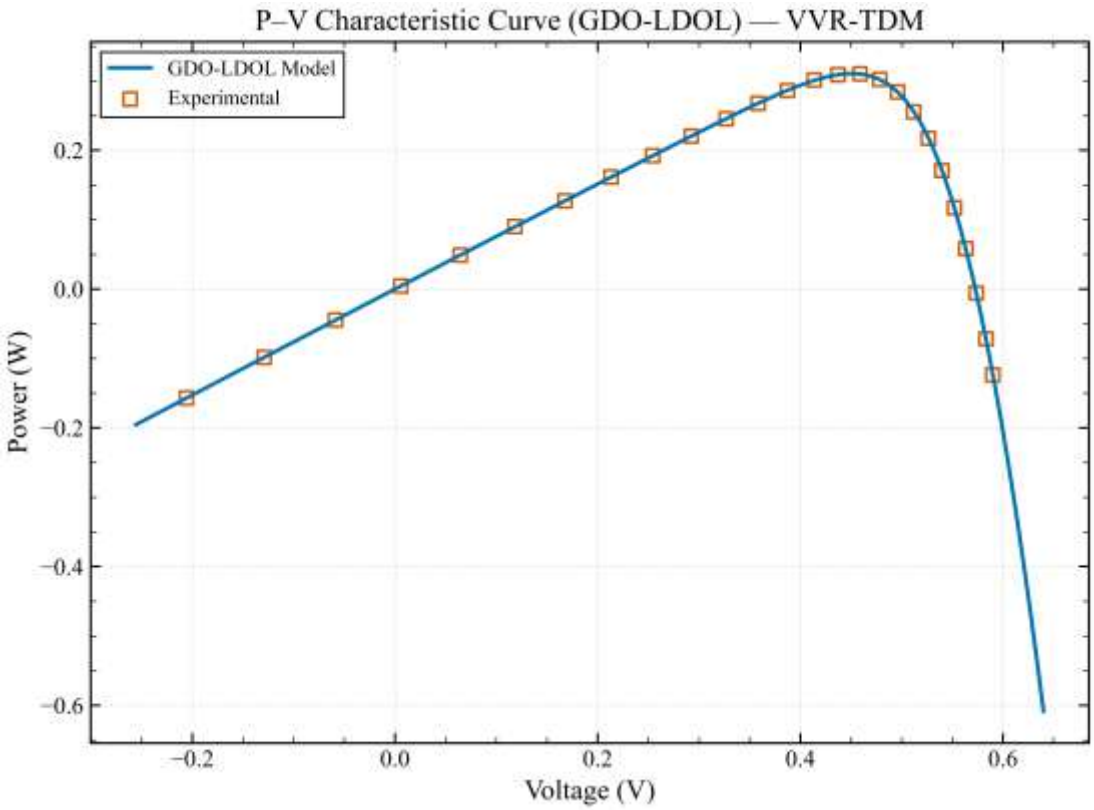


Figure 20. P–V Characteristics of the VVR-TDM for the GDO-LDOL (Best Run)

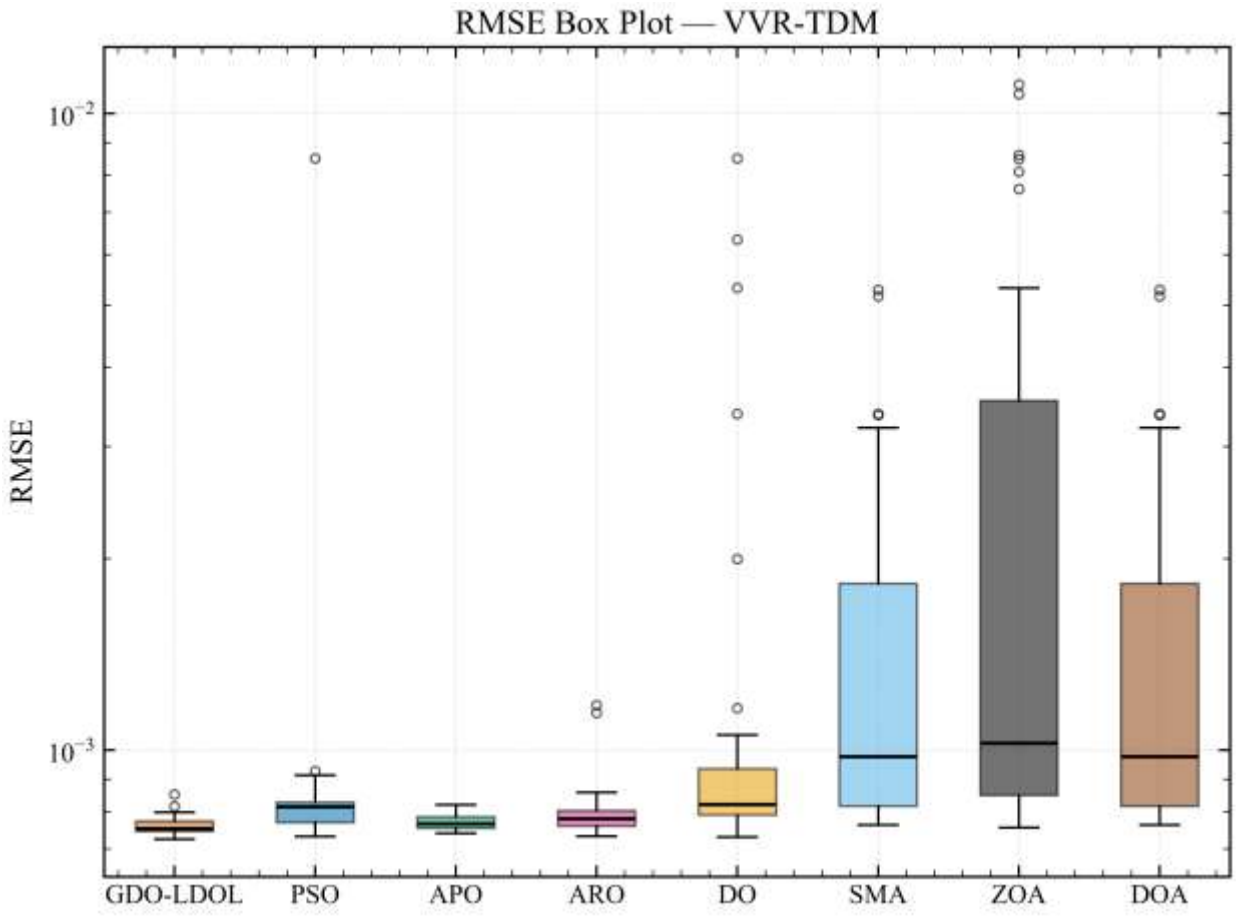


Figure 21. RMSE Boxplot of Optimization Algorithms for VVR-TDM (30 Runs).

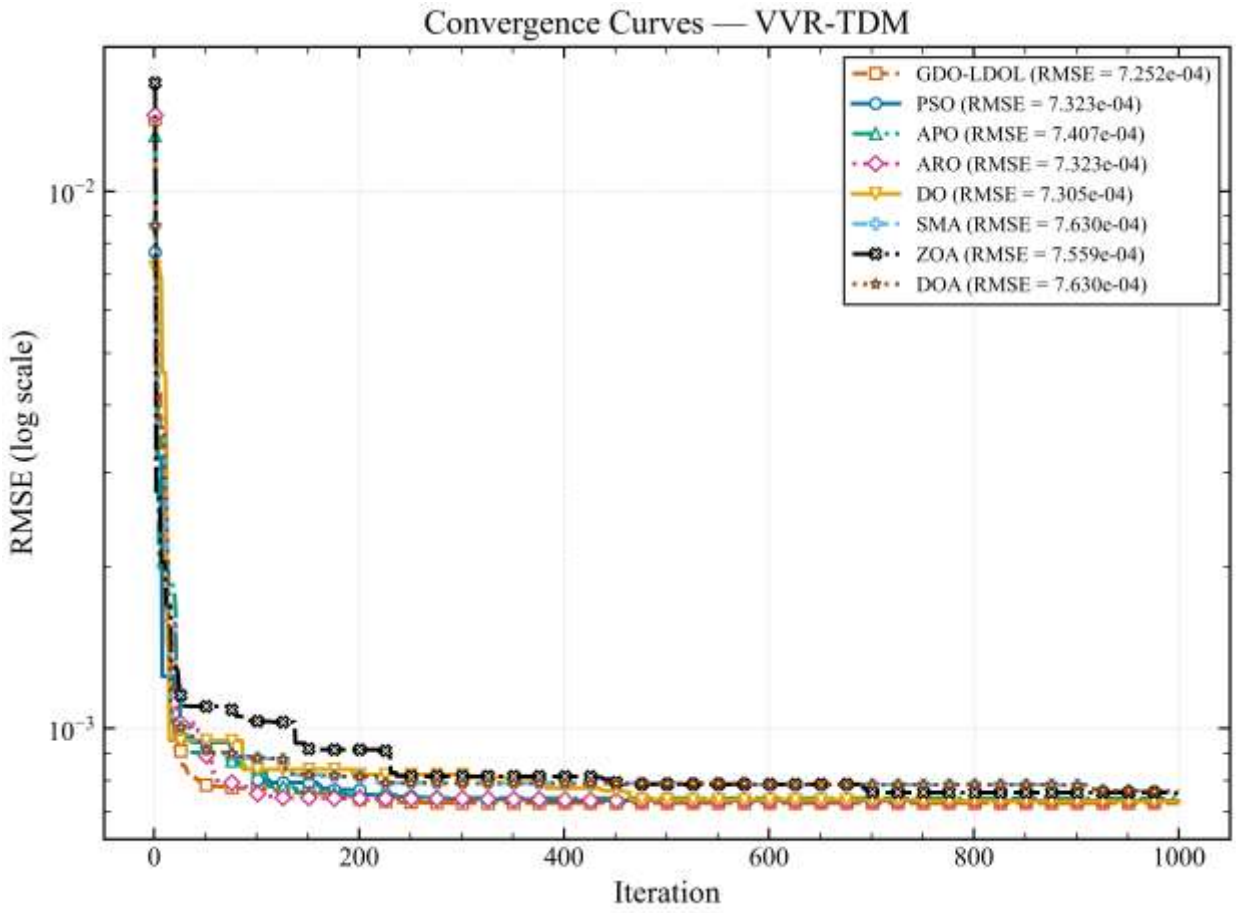


Figure 22. Convergence Curve for VVR-TDM via Optimization Algorithms (Best Run)

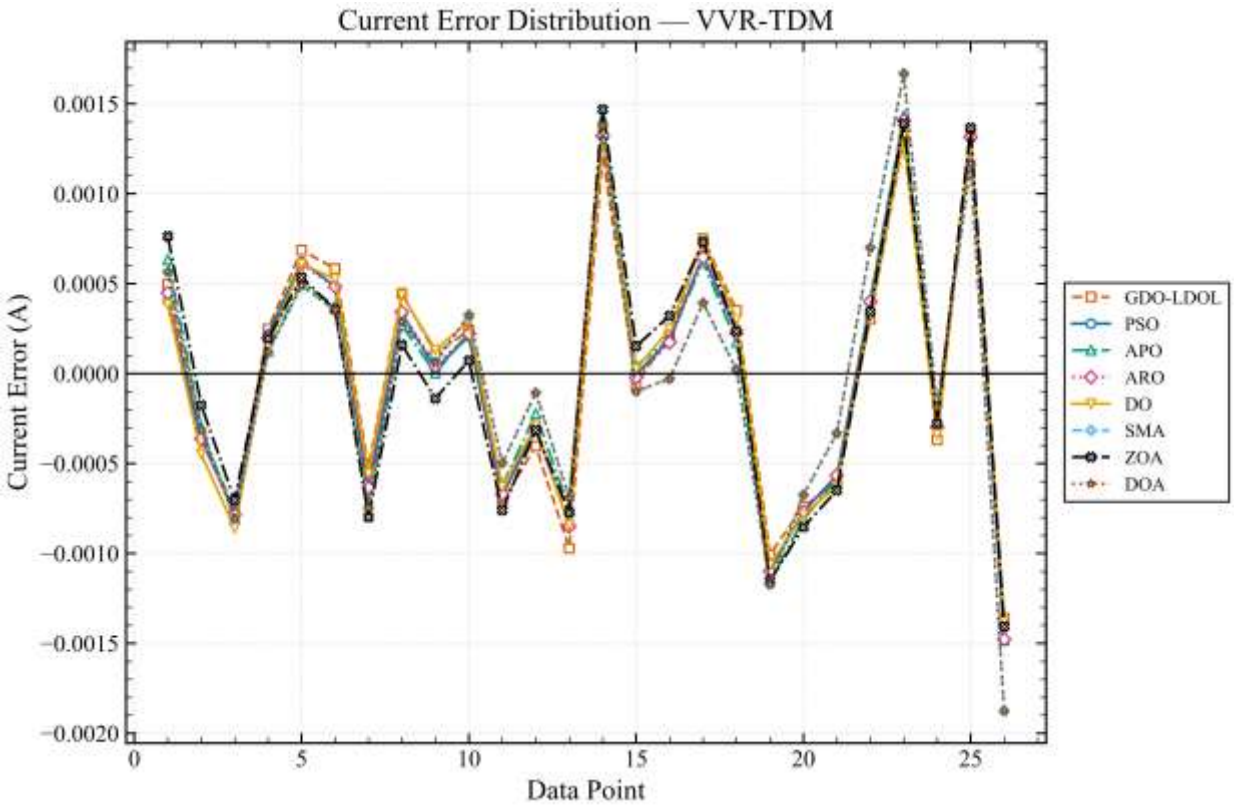


Figure 23. Current Error Distribution of Optimization Algorithms for VVR-TDM.

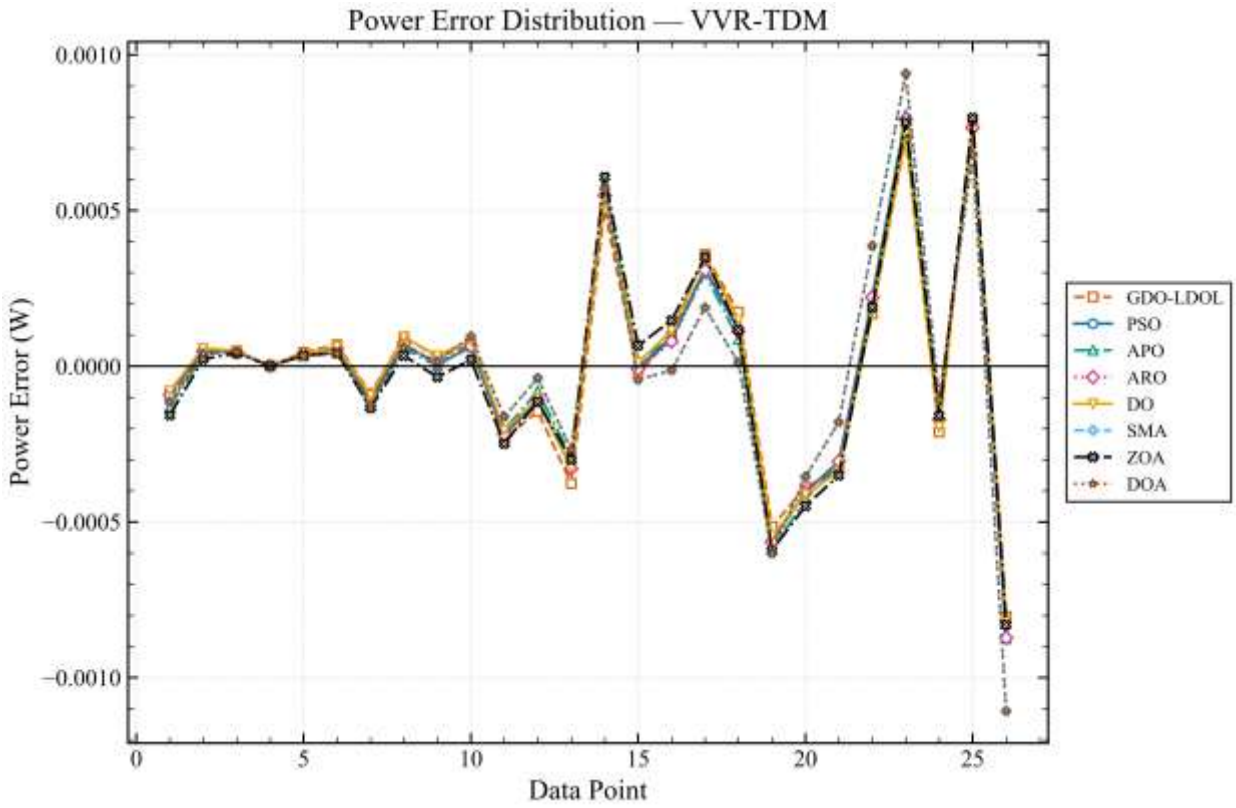


Figure 24. Power Error Distribution of Optimization Algorithms for VVR-TDM.

4.5. Comparative Discussion

The models are ranked by the minimum RMSE as follows: VVR-TDM (7.25×10^{-4}) < MTDM (7.41×10^{-4}) ≈ TDM (7.42×10^{-4}). The differences (about 2-3%) are small compared to the run-to-run spread of the weaker algorithms. The fit error alone does not establish the superiority of one model structure, because a model with more free parameters can be expected to reach a lower fit error simply because it has more freedom. Such a comparison would require a complexity penalized criterion (e.g. AIC or BIC) and independent validation data. However, the reliability of GDO-LDOL is high for all three models: its standard deviation is 2.43*10-4 for the TDM, 2.54*10-4 for the MTDM and 2.68*10-5 for the VVR-TDM, and its mean RMSE is 1.054*10-3, 1.044*10-3 and 7.62*10-4, respectively. GDO-LDOL is the only algorithm that achieves the top 2 rankings for both mean RMSE and standard deviation on all three models. The competing algorithms have model dependent weaknesses: PSO is unstable on the MTDM and also when combined with DO on the VVR-TDM; SMA, ZOA and DOA degrade considerably on the VVR-TDM; and DOA gives the poorest results on the TDM and MTDM, with a mean RMSE 5.7 and 6.0 times that of GDO-LDOL (2.2 times on the VVR-TDM).

These results agree with the design rationale of GDO-LDOL: the replacement of single-leader guidance by a dynamic similarity-fitness graph with a centrality-based hub reduces the risk of the whole population being collapsed onto one attractor, the Lévy -flight operator preserves long exploratory moves, and elitism, greedy selection, opposition-based learning and diversity restarts act as safeguards against loss of diversity. The experiments, however, do not separate the contribution of the individual components.

4.6. Limitations

The conclusions are restricted by the following. (i) Only one benchmark cell (26 I–V points at 303.15 K, 1000 W/m²) was used, and the model parameters were not validated with independent measurements. (ii) The comparison is based on descriptive statistics for 30 runs; no formal significance test was performed. (iii) GDO-LDOL has a cost of $O(T \cdot N^2 \cdot d)$ due to the graph construction, which is higher than the $O(T \cdot N \cdot d)$ of classical swarm methods, and the computation time was not compared. (iv) Several estimated parameters are at the limits of their search ranges, as noted above. The natural next steps are formal statistical testing, run-time measurements, an ablation study of the algorithmic components, and an evaluation on additional cells and modules under varing irradiance and temperature.

5. Conclusion

This paper proposed the Graph Dynamics Optimizer with Lévy Diffusion and Opposition Learning (GDO-LDOL), a population-based metaheuristic that embeds the search population in a dynamic, weighted similarity–fitness graph rather than following a single leader. A hybrid centrality measure identifies a hub agent, and each population member updates through either a Laplacian-diffusion/Lévy-flight exploration operator or a neighbourhood message-passing exploitation operator, with the balance annealed over the run and further stabilized by elitism, greedy selection, opposition-based learning, and diversity restarts. GDO-LDOL was validated on the R.T.C. France solar cell dataset for TDM, MTDM, and VVR-TDM, benchmarked over 30 independent runs against seven state-of-the-art optimizers (PSO, APO, ARO, DO, SMA, ZOA, DOA). It consistently achieved the lowest minimum RMSE across all three models (7.425×10^{-4}, 7.405×10^{-4}, and 7.252×10^{-4}, respectively), along with the best overall balance of accuracy and run-to-run stability, while several competing algorithms degraded sharply as model complexity increased. The close agreement between experimental and predicted I–V/P–V curves, together with physically consistent parameter esti-

mates, confirms the reliability of the proposed approach. These results support the core idea that structuring the population as a dynamic graph — rather than around a single global-best leader — improves robustness on the high-dimensional, multimodal landscapes of advanced diode models. Future work will extend GDO-LDOL to additional PV technologies and operating conditions, explore adaptive tuning of the graph hyperparameters (k, τ, p_r), and apply the framework to other engineering optimization problems such as MPPT controller tuning and battery parameter identification.

Author contributions

Conceptualization, Samah Elkholy, Ahmed Bayoumi and Wala Azab; Formal analysis, Wala Azab and Manal E. Ali; Investigation, Ahmed Bayoumi; Methodology, Ahmed Bayoumi and Arafa A. Nasif; Resources, Ahmed Bayoumi and Arafa A. Nasif; Software, Wala Azab; Validation, Ahmed Bayoumi and Manal E. Ali; Writing—original draft, Ahmed Bayoumi and Wala Azab; Writing—review & editing, Samah Elkholy, Manal E. Ali and Arafa A. Nasif. All authors have read and agreed to the published version of the manuscript.

Funding

This research received no external funding.

Competing interests

The authors declare no competing interests.

Data Availability

The datasets used and analyzed during the current study are included in the manuscript.

Code Availability

The code used to implement the proposed study is available from the corresponding author on reasonable request.

Additional information

Correspondence and requests for materials should be addressed to Ahmed Bayoumi

References

1. Kabeyi, M. J. B. & Olanrewaju, O. A. Sustainable Energy Transition for Renewable and Low Carbon Grid Electricity Generation and Supply. *Frontiers in Energy Research* vol. 9 Preprint at https://doi.org/10.3389/fenrg.2021.743114 (2022).

2. Spilnichenko, V., Khadzhiev, M. & Tarkhanova, Z. RENEWABLE ENERGY ECONOMY: POTENTIAL AND CHALLENGES. *Reliability: Theory and Applications* **19**, (2024).

3. Rezaee, E. & Silva, S. R. P. Solar Energy in 2025: Global Deployment, Cost Trends, and the Role of Energy Storage in Enabling a Resilient Smart Energy Infrastructure. *Energy and Environmental Materials* **9**, (2026).

4. K, P., Govindarajan, U., Ramachandaramurthy, V. K., T, S. O. S. & Jeevarathinam, B. Integrating solar photovoltaic energy conversion systems into industrial and commercial electrical energy utilization—A survey. *Journal of Industrial Information Integration* vol. 10 Preprint at https://doi.org/10.1016/j.jii.2018.01.003 (2018).

5. Yin, J., Zhu, Y. & Yu, G. Power transformer fault diagnosis based on support vector machine with cross validation and genetic algorithm. in *APAP 2011 - Proceedings: 2011 International Conference on Advanced Power System Automation and Protection* vol. 1 (2011).

6. Çelik, E. *et al.* Reconfigured single- and double-diode models for improved modelling of solar cells/modules. *Sci. Rep.* **15**, (2025).

7. Masita, K., Hasan, A., Shongwe, T. & Hilal, H. A. Deep learning in defects detection of PV modules: A review. *Solar Energy Advances* vol. 5 Preprint at https://doi.org/10.1016/j.seja.2025.100090 (2025).

8. Bayoumi, A. S. A., El-Sehiemy, R. A. & Abaza, A. Effective PV Parameter Estimation Algorithm Based on Marine Predators Optimizer Considering Normal and Low Radiation Operating Conditions. *Arab. J. Sci. Eng.* 1–16 (2021).

9. Mazhari, B. An improved solar cell circuit model for organic solar cells. *Solar Energy Materials and Solar Cells* https://doi.org/10.1016/j.solmat.2005.05.017 (2006) doi:10.1016/j.solmat.2005.05.017.

10. Bayoumi, A. S. A., El Sehiemy, R. A., El-Kemary, M. & Abaza, A. Advanced extraction of PV parameters' models based on electric field impacts on semiconductor conductivity using QIO algorithm. *Sci. Rep.* **14**, 1–13 (2024).

11. Tofallis, C., Horst, R., Padalos, P. M. & Thoai, N. V. Introduction to Global Optimization. *J. Oper. Res. Soc.* **47**, (1996).

12. Khan, S. B., Thilagavathy, R., Priyadarsini, K. & P J, A. L. R. A Survey On Non – linear Optimization And Global Optimization Methods. *International Journal of Computational Mathematics and Computer Science* **01**, (2024).

13. Das, A. *et al.* Metaheuristic Algorithms Since 2020: Development, Taxonomy, Analysis, and Applications. *Archives of Computational Methods in Engineering* Preprint at https://doi.org/10.1007/s11831-025-10408-3 (2025).

14. Bayoumi, A., Elbana, M. M., Nasaf, A. A. & Ali, M. E. A Novel Phantom Based Search Optimizer (PhaBSO) for Accurate Parameter Estimation of Photovoltaic Models. *Journal of Contemporary Technology and Applied Engineering* **5**, 1–30 (2026).

15. Nassereddine, K. & Turzynski, M. Demand response in DC microgrids using particle swarm optimization-optimized model predictive control. *Sci. Rep.* https://doi.org/10.1038/s41598-026-70019-1 (2026) doi:10.1038/s41598-026-70019-1.

16. Alam, T., Qamar, S., Dixit, A. & Benaida, M. Genetic algorithm: Reviews, implementations and applications. *International Journal of Engineering Pedagogy* vol. 10 Preprint at https://doi.org/10.3991/IJEP.V10I6.14567 (2021).

17. Yang, G., Sun, P., Zhang, J., Zhang, Y. & Li, T. An improved differential evolution algorithm based on reinforcement learning and its application. *Sci. Rep.* **15**, (2025).

18. Makhadmeh, S. N. *et al.* Recent Advances in Grey Wolf Optimizer, its Versions and Applications: Review. *IEEE Access* **12**, (2024).

19. Makhadmeh, S. N. *et al.* Recent advances in multi-objective whale optimization algorithm, its versions and applications. *Journal of King Saud University - Computer and Information Sciences* vol. 37 Preprint at https://doi.org/10.1007/s44443-025-00184-2 (2025).

20. Pham, V. H. S., Dang, N. T. N. & Nguyen, V. N. Advanced vehicle routing in cement distribution: a discrete Salp Swarm Algorithm approach. *International Journal of Management Science and Engineering Management* **20**, (2025).

21. Menesy, A. S., Sultan, H. M., Selim, A., Ashmawy, M. G. & Kamel, S. Developing and Applying Chaotic Harris Hawks Optimization Technique for Extracting Parameters of Several Proton Exchange Membrane Fuel Cell Stacks. *IEEE Access* **8**, (2020).

22. Agrawal, S. P. *et al.* The quick crisscross sine cosine algorithm for optimal FACTS placement in uncertain wind integrated scenario based power systems. *Results in Engineering* **25**, 103703 (2025).

23. Kalita, K., Pandya, S. B., Čep, R., Jangir, P. & Abualigah, L. Many-objective ant lion optimizer (MaOALO): A new many-objective optimizer with its engineering applications. *Heliyon* **10**, (2024).

24. Taher, M. A., Kamel, S., Jurado, F. & Ebeed, M. An improved moth-flame optimization algorithm for solving optimal power flow problem. *International Transactions on Electrical Energy Systems* https://doi.org/10.1002/etep.2743 (2019) doi:10.1002/etep.2743.

25. Chen, Y. & Wang, N. Cuckoo search algorithm with explosion operator for modeling proton exchange membrane fuel cells. *Int. J. Hydrogen Energy* **44**, (2019).

26. Yang, X. S. Bat algorithm: Literature review and applications. *International Journal of Bio-Inspired Computation* Preprint at https://doi.org/10.1504/IJBIC.2013.055093 (2013).

27. Anshory, I. *et al.* Optimization DC-DC boost converter of BLDC motor drive by solar panel using PID and firefly algorithm. *Results in Engineering* **21**, (2024).

28. Oliva, D., Cuevas, E. & Pajares, G. Parameter identification of solar cells using artificial bee colony optimization. *Energy* **72**, 93–102 (2014).

29. Abdel-Basset, M., Mohamed, R., Chakrabortty, R. K., Sallam, K. & Ryan, M. J. An efficient teaching-learning-based optimization algorithm for parameters identification of photovoltaic models: Analysis and validations. *Energy Convers. Manag.* **227**, (2021).

30. Djekidel, R. *et al.* Mitigating the effects of magnetic coupling between HV transmission line and metallic pipeline using slime mould algorithm. *J. Magn. Magn. Mater.* **529**, 167865 (2021).

31. Mohamed, E. A., Braik, M. S., Al-Betar, M. A., Yaseen, Q. M. & Shambour, Q. Y. Multi-strategy artificial protozoa optimizer for unconstrained functions, engineering problems, and feature selection. *Neural Comput. Appl.* **38**, (2026).

32. Bayoumi, A. S. A. *et al.* Optimizing Multi-Layer Perovskite Solar Cell Dynamic Models with Hysteresis Consideration Using Artificial Rabbits Optimization. *Mathematics* **11**, (2023).

33. Saglam, M., Bektas, Y. & Karaman, O. A. Dandelion Optimizer and Gold Rush Optimizer Algorithm-Based Optimization of Multilevel Inverters. *Arab. J. Sci. Eng.* **49**, (2024).

34. Li, C., Wang, X., Zhang, Q., Liang, J. & Zhang, A. DDoS Attack Autonomous Detection Model Based on Multi-Strategy Integrate Zebra Optimization Algorithm. *Computers, Materials and Continua* **82**, (2025).

35. Lang, Y. & Gao, Y. Dream Optimization Algorithm (DOA): A novel metaheuristic optimization algorithm inspired by human dreams and its applications to real-world engineering problems. *Comput. Methods Appl. Mech. Eng.* **436**, (2025).

36. Mangaiyarkkarasi, J., Revathy, J. S. & Mehta, S. Introduction to graph theory. in *Neural Networks and Graph Models for Traffic and Energy Systems* (2025). doi:10.4018/979-8-3373-0290-4.ch003.

37. Yin, H., Yang, S., Wen, X., Wang, H. & Yang, S. Spatial patterns of the Brusselator model with asymmetric Lévy diffusion. *Chinese Physics B* **33**, (2024).

38. Bayoumi, A. S., El-Sehiemy, R. A., Mahmoud, K., Lehtonen, M. & Darwish, M. M. F. Assessment of an improved three-diode against modified two-diode patterns of MCS solar cells associated with soft parameter estimation paradigms. *Applied Sciences (Switzerland)* **11**, (2021).

39. Chen, Y. G. *et al.* Differential evolution with classified mutation for parameter extraction of photovoltaic models. *PLoS One* **20**, (2025).

40. Hali, A. & Khlifi, Y. Fast and Efficient Way of PV Parameters Estimation Based on Combined Analytical and Numerical Approaches. *Applied Solar Energy (English translation of Geliotekhnika)* **59**, (2023).